nature ecology & evolution

Article

https://doi.org/10.1038/s41559-024-02551-0

Warming and disturbances affect Arctic-boreal vegetation resilience across northwestern North America

Received: 17 December 2023

Accepted: 3 September 2024

Published online: 8 October 2024

Check for updates

Yue Zhang[1], Jonathan A. Wang[2], Logan T. Berner[3], Scott J. Goetz[3], Kaiguang Zhao[4] & Yanlan Liu[1,4]

Rapid warming and increasing disturbances in high-latitude regions have caused extensive vegetation shifts and uncertainty in future carbon budgets. Better predictions of vegetation dynamics and functions require characterizing resilience, which indicates the capability of an ecosystem to recover from perturbations. Here, using temporal autocorrelation of remotely sensed greenness, we quantify time-varying vegetation resilience during 2000–2019 across northwestern North American Arctic-boreal ecosystems. We find that vegetation resilience significantly decreased in southern boreal forests, including forests showing greening trends, while it increased in most of the Arctic tundra. Warm and dry areas with high elevation and dense vegetation cover were among the hotspots of reduced resilience. Resilience further declined both before and after forest losses and fires, especially in southern boreal forests. These findings indicate that warming and disturbance have been altering vegetation resilience, potentially undermining the expected long-term increase of high-latitude carbon uptake under future climate.

Arctic and subarctic regions (hereafter 'Arctic-boreal') have warmed several times faster than the global average since the mid-twentieth century, with further rapid warming projected in the coming decades[1,2]. Warmer temperatures are widely promoting vegetation productivity (that is, 'greening'), thereby contributing to increased carbon sink capacity in northern high latitudes[3–6]. However, rapid warming is also accompanied by climate stresses and disturbances, including droughts, permafrost degradation, fires and insect outbreaks[7–9]. Consequently, Arctic-boreal vegetation exhibited heterogeneous greening and browning trends along with extensive land-cover changes (LCCs) in recent decades[10–13]. Multiscale observations have documented shrub expansion in Arctic tundra[14], boreal forest losses[9,15] and composition shifts post disturbance[16]. Pervasive vegetation changes have profound yet uncertain impacts on carbon dynamics[10,17–19], energy budgets[20,21], ecological stability[16] and climate feedbacks[14]. For example, while Earth system models typically project increased Arctic-boreal biomass and productivity over the coming decades, the associated uncertainties are three times the global average change, in part due to underconstrained vegetation changes[22]. Long-term changes in Arctic-boreal ecosystem functions depend not only on the greening and browning trends but also on the trajectories of intermittent and abrupt vegetation shifts and the recovery rate afterwards. Thus, predicting the abrupt changes and their consequential impacts requires understanding ecological resilience, that is, when and where vegetation becomes vulnerable to climate stress and disturbance with a high propensity to cross the tipping point of enduring vegetation shift[23].

Ecological resilience measures the capacity or rate of a system to recover from deviated states[24–27]. Here, we define vegetation resilience as the recovery rate from deviations caused by perturbations to the equilibrium state. Low resilience before vegetation loss reflects slow

[1]School of Earth Sciences, The Ohio State University, Columbus, OH, USA. [2]School of Biological Sciences, University of Utah, Salt Lake City, UT, USA. [3]School of Informatics, Computing, and Cyber Systems, Northern Arizona University, Flagstaff, AZ, USA. [4]School of Environment and Natural Resources, The Ohio State University, Columbus, OH, USA. e-mail: liu.9367@osu.edu

https://doi.org/10.1038/s41559-024-02551-0

recovery from subtle anomalies of biomass or greenness, possibly due to impaired ecophysiological capability to repair partial damage. This indicates increased vulnerability to further climate perturbations and thus increased likelihood of approaching a tipping point where abrupt loss may occur[28–30]. Such an early warning signal has been found useful in predicting temperate and tropical forest losses[28,31]. After LCCs or disturbances, low resilience reflects restricted recovery capability to the new equilibrium state[16,32], possibly dampening the ecosystem carbon sink[16,33,34]. Observational studies have measured boreal forest resilience by comparing observed growth, density and composition after droughts and fires to those predisturbance[16,34,35]. These metrics, however, mostly measure resilience after disturbance events, with the exception of diagnosing radial growth before disturbance or forest loss using tree-ring records[30,36,37] and are limited by spatial-temporal coverage. Diagnosing resilience, including that before abrupt changes, requires a broader scope entailing the ability to recover from pulse disturbances such as acute droughts and fires but also press disturbances related to more gradual changes in climate variables, such as temperature and long-term moisture availability[38,39]. Doing so allows detecting ecosystems exhibiting increased vulnerability and lowered capacity to withstand ecosystem degradation or conversion.

Low resilience is linked with high lag-1 temporal autocorrelation (the correlation between values that are one time step apart) of system state variables such as biomass or greenness according to nonlinear dynamical theories[27,40]. Recent studies have applied such theories to estimate vegetation resilience change over large areas using decadal-scale satellite-observed vegetation indices, for example, the normalized difference vegetation index (NDVI) or vegetation optical depth (VOD)[26,41,42]. The rationale behind this approach is that high autocorrelation indicates slow recovery from anomalies due to changes in vegetation photosynthetic capacity, thereby leaving the ecosystem less capable of withstanding further perturbations. For example, slow recovery has been linked to reduced growth, hydraulic impairment and depletion of non-structural carbon storage under drought stress before abrupt losses[30,37,43]. The existing regional to global studies have suggested reduced resilience in the tropics and arid temperate forests, in contrast to mixed but generally enhanced resilience in Arctic-boreal regions in response to climate change[26,41,42,44]. However, the coarse (5–25 km) spatial resolutions of the existing studies hindered investigating resilience at ecologically relevant scales and assessing a multitude of fine-scale environmental controls of resilience trends. In addition, unlike resilience before vegetation change, applications of using lag-1 autocorrelation to evaluate resilience after regime shifts, such as vegetation loss, have been rare; however, theoretical analyses have demonstrated its effectiveness in measuring the recovery rate to the new equilibrium state[45–47]. Applying the theory to observed data requires a method that allows adaptive estimation of lag-1 autocorrelation while considering shifted equilibrium state, which will allow explicitly diagnosing resilience variation both before and after abrupt changes. Doing so is essential for deriving mechanistic understanding on the factors driving the emerging resilience signal and leveraging remotely sensed resilience to better predict vegetation changes and their impacts on the global carbon cycle.

Here, we address this knowledge gap by focusing on vegetation dynamics across the NASA Arctic-Boreal Vulnerability Experiment (ABoVE) core domain, mainly Alaska and northwestern Canada, during 2000–2019, when resilience changed more prominently than in earlier decades due to increased wildfires and climate warming[42]. Previous studies have developed rich datasets quantifying climate change, disturbances, LCC and multiple environmental conditions in this area, offering an ideal testbed to address the following questions[7,11]: (1) What were the spatial-temporal patterns of Arctic-boreal vegetation resilience change? (2) What environmental conditions could explain the change patterns? (3) How did resilience vary before and after LCCs or fire disturbances? To quantify resilience, we used vegetation greenness

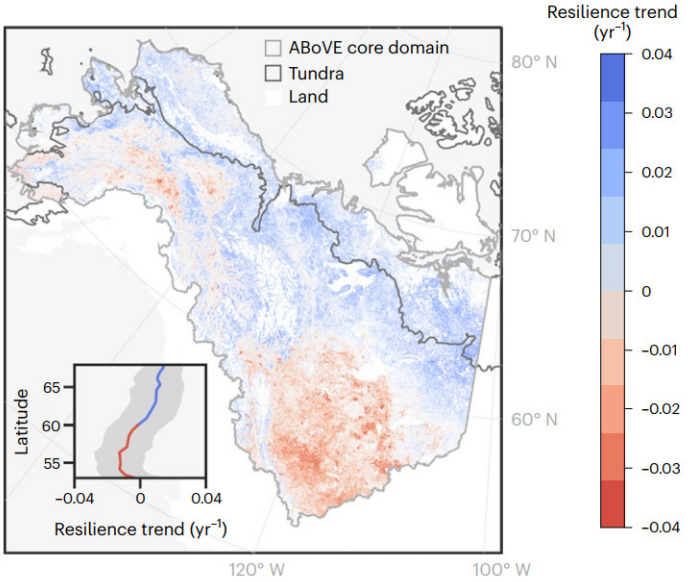

Fig. 1 | Vegetation resilience pervasively decreased in southern boreal forests while increased in Arctic tundra. The map shows the trend of resilience (posterior mean) from 2000 to 2019 across the ABoVE core domain. Only areas showing significant trend (two-sided *t*-test $\alpha = 0.05$) are coloured. The inset shows the latitudinal variation of resilience trend with a bin size of 0.75°, where the line and grey band denote the mean and the standard deviation, respectively. Darker grey polygons delineate the boundaries of Arctic tundra based on ecoregions of North America from the US Environmental Protection Agency. Areas with low availability of valid data, dominance of water bodies or non-significant resilience trend are shown in white.

as the state variable, measured by the enhanced vegetation index (EVI) from the moderate resolution imaging spectroradiometer (MODIS) at a 300 m spatial resolution and a 16-day temporal resolution[48]. We first estimated time-varying lag-1 autocorrelation of EVI with a 16-day interval using a Bayesian dynamic linear model (DLM), which disentangles autocorrelation from concurrent signals arising from trend, changing equilibrium state and climate forcings (Extended Data Figs. 1 and 2)[28,49]. Because a high autocorrelation indicates low resilience[26,40–42], we used the posterior mean of negative lag-1 autocorrelation of EVI as a proxy of vegetation resilience. We quantified long-term trend of resilience across the domain and identified environmental factors controlling its spatial pattern for areas without LCC or recorded disturbance. We then focused on areas that experienced climate-driven LCCs or fire disturbance to characterize annual resilience variation before and after these abrupt changes. We found that resilience pervasively increased in Arctic tundra but decreased in southern boreal forests. Reduced resilience was mostly likely to occur in warm, dry, high elevation environments with dense vegetation cover and was further exacerbated by LCCs and fire disturbance. Reduced resilience probably undermines the projected productivity increase in the coming decades with continued climate warming.

Spatial and temporal pattern of vegetation resilience

Boreal forests with high tree cover experienced extensive resilience declines, at fast rates in interior Alaska and the southeast portion of the domain (Fig. 1 and Extended Data Fig. 3). In contrast, the Arctic tundra exhibited widespread resilience increases. Across the latitudinal gradient, the average resilience reduced at faster rates at lower latitudes, switching from positive to negative trends at ~61° N (Fig. 1). Throughout the 3.6 M km^2 domain, resilience significantly increased in 56% of the vegetated area, while it significantly decreased in 36% during 2000–2019 (two-sided *t*-test $\alpha = 0.05$) (Fig. 2). The large areal fraction

https://doi.org/10.1038/s41559-024-02551-0

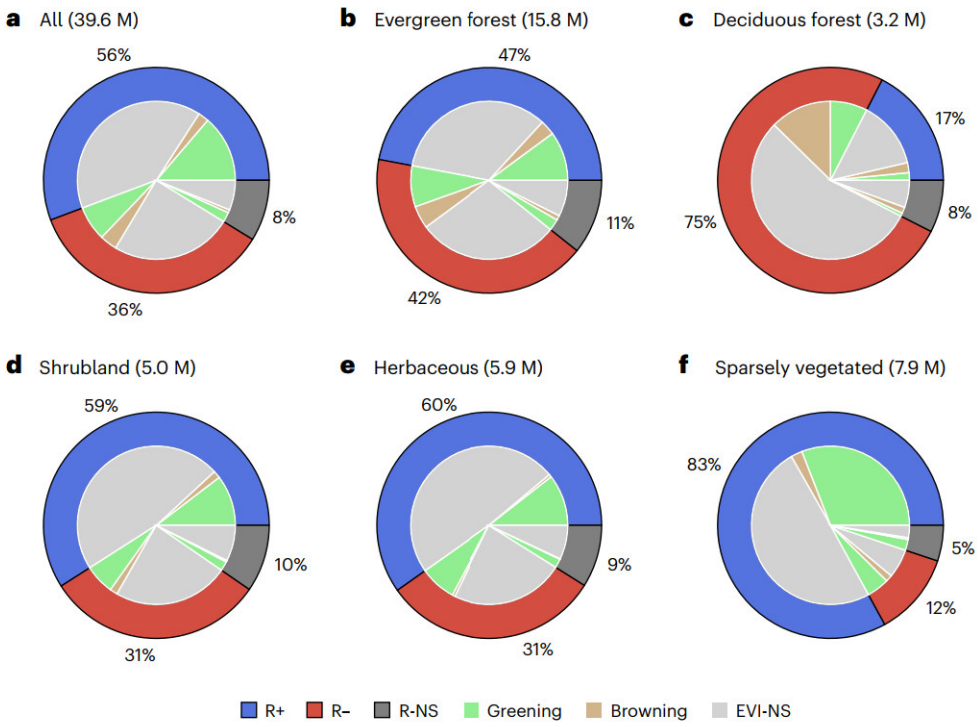

Fig. 2 | Greening does not always enhance vegetation resilience. a–f, The outer pie shows the areal fractions of significantly (two-sided *t*-test $\alpha = 0.05$) increased (R+), significantly decreased (R−) and non-significant (R-NS) resilience trend among all vegetated areas (**a**) and the major land-cover types, including evergreen forest (**b**), deciduous forest (**c**), shrubland (**d**), herbaceous (**e**) and sparsely vegetated (**f**). The nested inner pie shows the areal fractions of significant greening, browning and non-significant (EVI-NS) greenness trend within each resilience trend group (outer pie). The number of pixels in each panel is noted in round brackets.

of significant resilience trends benefited from the Bayesian model, which can disentangle the autocorrelation signal from other components blended in the time series (Methods). Among the five major land-cover types, deciduous forest experienced the most pervasive resilience decline (75% of deciduous forest area) followed by evergreen forest (42% of evergreen forest area). By contrast, only 12% and 31% of sparsely vegetated and herbaceous areas showed resilience decline.

Notably, the spatial pattern of resilience trends is not always consistent with that of greenness trends. Vegetation greenness significantly increased (greening) in 23% of the domain and decreased (browning) in 6% of the domain, while the remaining showed no significant trend during 2000–2019 (Fig. 2). Most (56%) browning areas experienced reduced resilience. However, a substantial fraction (31%) of greening areas also showed reduced resilience, especially in boreal forests (Extended Data Fig. 3). More than 40% of greening evergreen forest and >76% of greening deciduous forest showed reduced resilience. A similar pattern holds when excluding areas with recorded LCC or disturbances (Extended Data Fig. 4). These results highlight that, although greening is expected to indicate enhanced productivity and biomass[3,6,10], it does not always enhance vegetation resilience, potentially predisposing these forests to more substaintial losses due to future climate stress.

Environmental controls on vegetation resilience change

To investigate what environmental factors affect resilience trends, we built a random forest classification model to explain the sign of resilience change for areas without LCC or recorded disturbance during 2000–2019. The predictors include climate, permafrost, topography, land cover, soil moisture and soil nitrogen. These factors explained 81.4% [80.7%, 82.1%] of the spatial variation in the sign of resilience change [95% confidence interval]. Vegetation resilience was most likely to decrease in areas with high summer air temperature, deep active layer thickness (ALT), high elevations, dry winters with low precipitation as snow, high summer EVI, low soil nitrogen content and dry summers with high climate moisture deficit (Fig. 3). Notably, factors representing aboveground (summer air temperature) and belowground (ALT) temperature were the most important in explaining resilience change. Resilience was more likely to decrease if long-term average summer air temperature was >12.5 °C or if ALT was deeper than 1.5 m. Compounded with high temperature, limited moisture supply as measured by low precipitation as snow (<180 mm) and high summer climate moisture deficit (>40 mm) further contributed to resilience reduction. Resilience also tended to reduce in areas with dense vegetation cover compounded with low soil nitrogen availability, which is indicative of nutrient limitation[50,51]. Conversely, resilience change was minimally explained by the trend of summer EVI or land-cover type, indicating that the reduced resilience was not specific to greening/browning areas or a given plant type but primarily regulated by thermal, moisture and nitrogen regimes.

Resilience before and after LCC or fire

After climate-driven LCCs (changes not caused by recorded fire, logging or insects[7,52]) and fires, the growing season EVI exhibited heterogeneous variations, reducing in 45% of forest loss areas and 61% of fire-disturbed areas 5 years after (Extended Data Fig. 5). The changed EVI was used to estimate the shifted equilibrium states in the Bayesian DLM and the corresponding resilience after changes (Methods). We further examined how the emergent resilience trajectories were affected by the abrupt changes by comparing to the baseline resilience unaffected by the changes. We calculated the fractions of pixels experiencing resilience lower than the baseline between 5 years before and after the abrupt changes (Methods; examples in Supplementary Fig. 1). Focusing on areas with LCC, 76% and 82% of deciduous forest

https://doi.org/10.1038/s41559-024-02551-0

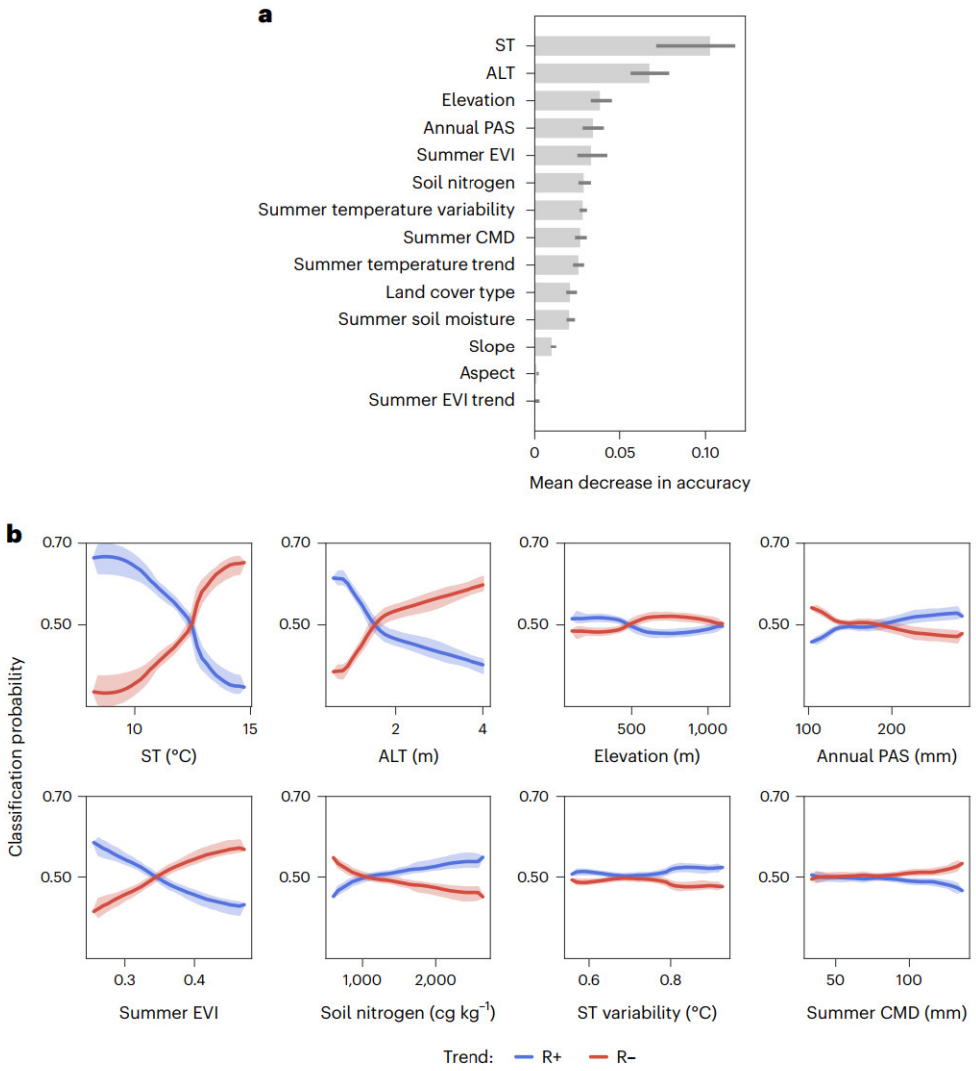

Fig. 3 | Vegetation resilience was more likely to decline in warm, dry regions with deep active layers, high elevation, high greenness and low soil nitrogen. **a**, The relative importance of environmental factors predicting the direction of vegetation resilience change. A larger mean decrease in accuracy indicates greater importance. The bar height and the error bar show the median and the 95% uncertainty intervals of mean decrease in accuracy across 100 simulations, respectively. **b**, Partial dependence plots illustrating the response of the classification probability to each of the top eight predictors. The lines and bands indicate the medians and the 95% uncertainty intervals across 100 simulations for the probability of increasing (R+) and decreasing (R−) resilience, respectively. ST, summer temperature; ALT, active layer thickness; PAS, precipitation as snow; CMD, climate moisture deficit.

losses were preceded by reduced resilience 3 and 1 years before, respectively (Fig. 4a). Evergreen forest loss was only frequently preceded by reduced resilience on the southern edge of the study domain (Fig. 4b). Resilience also reduced in shrublands or non-woody ecosystems before being colonized by deciduous forests. The reduced resilience provided early warnings before the changes, with stronger signals at shorter lead times. The early warning was probably contributed by impaired ecophysiological functions under moisture stresses, which were typically severer during the low-resilience periods than the long-term averages (Supplementary Fig. 2). Notably, forest losses led to persistently low resilience afterwards. By contrast, shrub gain, which primarily occurred in Arctic tundra, contributed to enhanced resilience both before and after. Consistent across all the LCC types, resilience reduced more frequently in lower latitudes (Fig. 4b).

After fires, most evergreen forests (74%) and deciduous forests (89%) remained at low resilience 5 years after, suggesting limited recovery within 5 years postfire, especially in forests compared to non-forests (Fig. 4c). Given that more areas exhibited low resilience after fires (Fig. 4c) than after LCC (Fig. 4a), fires probably impaired ecosystem resilience more than climate stress alone. Nevertheless, as reflected by the variability across and within the latitudinal groups (Fig. 4d), postfire resilience was probably modulated by complex interactions such as among fire severity and postfire climates. To account for different ecosystem dynamics after LCC and fires, we also tested intervening the Bayesian inference at the time of change by reducing the weight of prior knowledge learned from observations before the change while mostly relying on limited number of new observations afterwards to estimate resilience (Methods). The results show substantial uncertainty in the aggregated fraction of resilience reduction especially within 3 years after LCC and fires due to limited observations (Extended Data Fig. 6). However, the reduction of resilience 5 years after remains robust in lower latitudes. Thus, while further research is needed to evaluate the heterogeneous patterns and uncertainties of resilience trajectories, the consistent finding that LCC and fire disturbances were frequently accompanied by reduced resilience highlights their prominent impacts on diminishing ecosystem resilience on the southern edge of the domain. Results showing F(R−) calculated by comparing resilience in the target year to the spatial baseline are in Extended Data Fig. 7.

https://doi.org/10.1038/s41559-024-02551-0

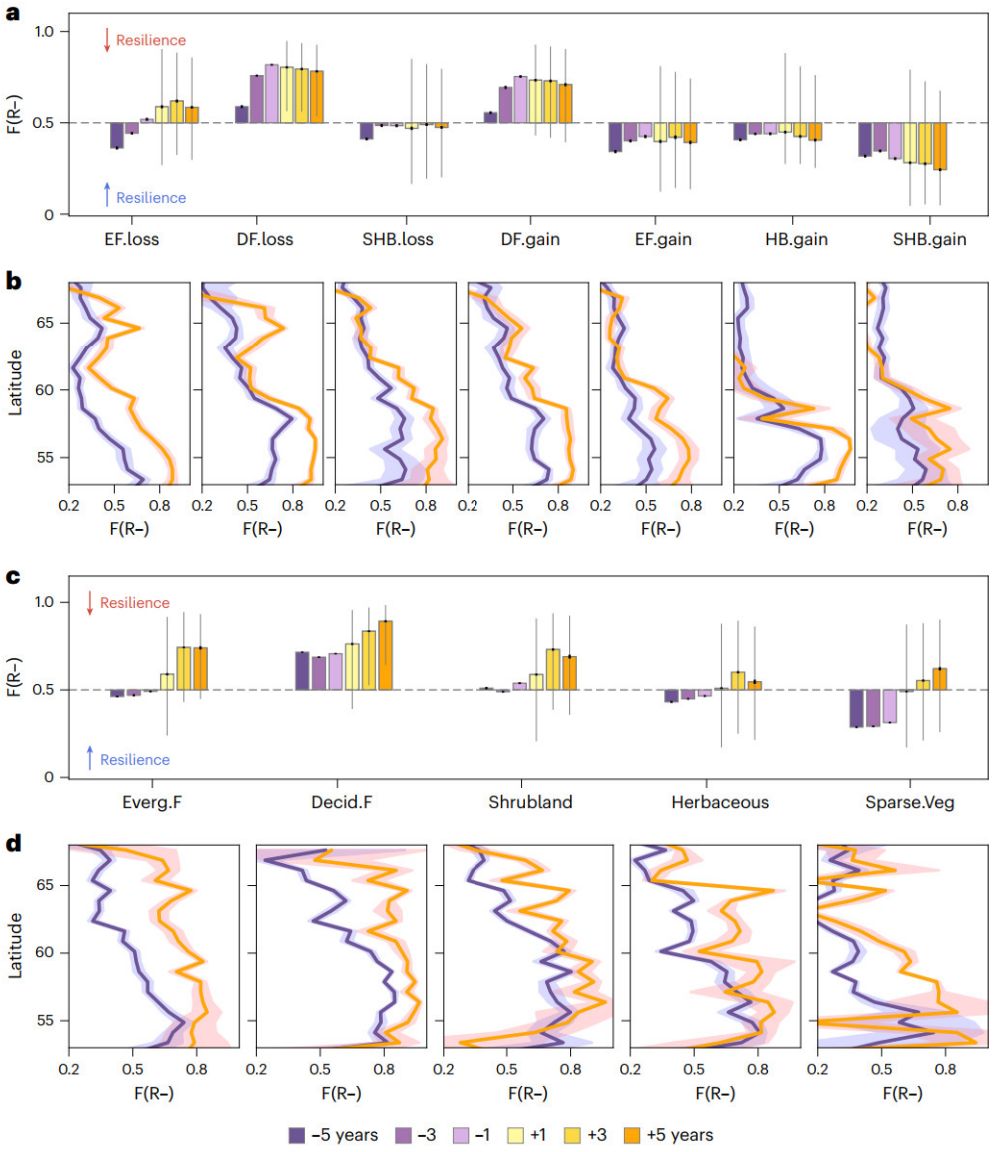

Fig. 4 | LCCs and fires were frequently accompanied by reduced resilience. **a**, The fraction of resilience lower than the baseline (F(R−)) between 5 years before and after climate-driven LCC, grouped by LCC types; that is, evergreen forest loss (EF.loss), deciduous forest loss (DF.loss), shrub loss (SHB.loss), deciduous forest gain (DF.gain), evergreen forest gain (EF.gain), herbaceous gain (HB.gain) and shrub gain (SHB.gain). An F(R−) >0.5 indicates that most pixels in this group experienced reduced resilience. **b**, The latitudinal variation of F(R−) grouped by a bin size of 0.75° for each LCC type. **c**,**d**, F(R−) before and after fires grouped by the prefire land-cover types (**c**) and the corresponding latitudinal variation (**d**), similar to **a** and **b**. The colours represent 5 years before (−5) and after (+5) the LCC or fire and so forth. F(R−) was calculated by comparing resilience (posterior mean) in the target year to the temporal baseline; that is, the resilience at the same location averaged between 2003 to 5 years before changes. The bar height in **a** and **c** is the mean F(R−) across 100 sets of bootstrapping pixels for each group (n = 10,000 for each set). The thick black vertical line shows the standard deviation, suggesting robust estimates across sampled pixels. The lower/upper end of the thin grey vertical line is F(R−) quantified by comparing the upper/lower boundary of resilience (posterior mean ± posterior standard deviation) to the abovementioned baseline, indicating large posterior range of resilience estimates post changes. The lines and shaded bands in **b** and **d** show the mean and standard deviation of F(R−) from 100 bootstrap resampling.

Discussion

We found that the resilience of Arctic tundra benefited more from recent warming than boreal forest did. This is probably due to alleviated constraints of temperature and resultantly nutrient availability on growth, establishment and post-disturbance recovery of tundra vegetation[14,51,53,54]. Nitrogen-fixing shrubs can increase the nitrogen inputs and create a positive feedback for shrub gain[55]. As a result, steadily enhanced tundra vegetation growth and shrub gain could enhance ecosystem productivity and structural diversity, thereby hypothetically contributing to enhanced ecosystem resilience (Fig. 4a)[14,56]. In boreal forests, although a previous global analysis covering southeastern Canada and Eurasia suggested increased boreal forest resilience[41], our results indicate generally reduced resilience in western Canada and interior Alaska, especially in areas with high heat and moisture stresses. This contrast probably arises from the strong impact of droughts on boreal forest resilience and different methods used to calculate lag-1 autocorrelation. To evaluate the impact of the methods, we replicated the method used in the previous global analysis using our data and found similarly increasing resilience in parts of the southeastern domain[41]. However, the replicated spatial pattern showed much greater spatial heterogeneity probably due to a higher data resolution used here and substantial estimation uncertainty

due to large fractions of missing EVI data and uncertainties in the estimated climate-induced autocorrelation—two challenges more prominent within the domain than at a global scale (Extended Data Fig. 8). The difference highlights that resilience estimates depend on the choice of methods and study domains. The Bayesian DLM here produced robust estimates relatively insensitive to specific values of posterior ranges and model hyperparameters (Extended Data Figs. 9 and 10), benefiting from joint estimation of autocorrelation and climate impact without interpolating missing data, which is known to introduce artifacts into autocorrelation estimates[57]. The pervasive resilience trends inferred from the Bayesian model (Supplementary Method 2) suggest prominent changes in vegetation resilience over the recent decades, while future work is needed to further examine the effectiveness of remote sensing derived resilience metrics by relating it to ground observed ecological transitions and recovery types. We note that uncertainty exists in the divide between enhanced and reduced resilience across the latitudes due to posterior uncertainty of the estimated autocorrelation and the information discounting parameter in the Bayesian model (Extended Data Figs. 9 and 10). However, the contrasting pattern between tundra and boreal forest regions is robust, with higher confidence in the declining resilience of boreal forests than the enhanced resilience of tundra vegetation.

The results of the resilience change pattern and its response to environmental conditions (Fig. 3) are supported by previous experiments and field observations[16,34,50,54,58,59]. Patterns of resilience reduction conform with drought-induced browning[12], reduced productivity[60], limited radial growth[61] and mortality[9,15], which have already been increasingly detected in boreal forests of northwestern North America, particularly on the warmer and drier extents of the biome. Specifically, previous observations suggested that warming probably inhibited tree growth in southern boreal forests, especially those with limited moisture supply[58], which is in line with pervasive resilience decline in warm and dry boreal forests found here. Remote sensing revealed that postfire recovery of tree cover was much slower in the south than in the north of North American boreal forests[59], supporting the latitudinal gradient of postfire resilience (Fig. 4d). Furthermore, deeper active layers have been found not to sustain boreal productivity in the long-term but could promote drainage and make boreal forests more susceptible to drought[62]. Resilience decline with soil nitrogen is also supported by observations suggesting that nutrients limited productivity and postfire recovery in the already nutrient-limited Arctic-boreal ecosystems[50,54]. Despite Earth system model projections of increasing Arctic-boreal carbon sink, driven by enhanced boreal forest productivity under warming and CO_2 fertilization[19,63], the expected long-term carbon sink will probably be dampened with declining resilience in southern boreal forests in northwestern North America with large biomass and productivity[19,63,64]. This is because reduced resilience implies a higher likelihood of crossing a threshold of forest loss—as supported by the results reported here (Fig. 4) and in other ecosystems[28,31]—and a limited capability to recover afterwards. As boreal forests are generally less resilient to drought compared to other ecosystems due to low species richness[65], declining resilience under future warming and droughts may further impair their stability[8].

Our findings suggest that greening does not always enhance resilience (Fig. 2). Increased greenness is positively correlated with radial growth, productivity, biomass and tree and shrub expansion[10,66,67], which could in theory allow greater capacity to absorb climate perturbations. Although we indeed found that greening co-occurred with increased resilience more frequently than browning did, greening also frequently co-occurred with reduced resilience in boreal forests (Extended Data Fig. 4). Spatial discrepancy between greening and enhanced resilience was also found in China's loess plateau[68]. This could partially be attributable to the fact that ecosystem degradation to herbaceous land covers may also exhibit greening[66]. Additionally, the contrast implies that greening in these areas may not be sustained in the long term, subject to a higher likelihood of changing land cover or productivity changes associated with shifting biomes. This hypothesis is supported by previous findings indicating that Arctic-boreal ecosystems are hotspots of structural overshoot[69,70]. That is, periods with favourable climates could temporarily enhance growth, leading it to surpass the longer-term environmental carrying capacity, thus making the ecosystem more vulnerable to climate stresses. Future work is required to assess the spatial correspondence of resilience decline with structural overshoot. Collectively, assessing future Arctic-boreal vegetation change and its implications on carbon budget requires considering both the transient trends of greening/browning and the likelihood of abrupt biome shifts reflected by resilience to perturbations.

Several types of climate-driven LCCs were preceded by reduced resilience, an early warning of vegetation shifts (Fig. 4a and Extended Data Fig. 7a). More often than not, forests that experienced climate-driven loss exhibited abnormally low resilience 1–5 years before, particularly in the southern boreal forests, a lead time comparable to that identified for drought-induced temperate forest loss[28]. Given that multiple ecosystem regimes varying from treeless to forest co-exist under similar boreal climate, reduced resilience offers a promising tool to predict abrupt biome transitions[71]. The occurrence of early warning requires long legacy effects of acute stress or chronic stress which slowly impairs ecophysiological functions, supported by multiscale studies in high-latitude ecosystems[72–75]. For example, measurements of southern Eurasian boreal forest species suggested that short-term exposure to extreme heat during summer could cause long-term damage to plant photosynthetic apparatus, which may trigger large-scale forest loss in succeeding years[76]. Warming experiments further suggested that even modest warming could substantially limit boreal species recruitment and survival, indicating potential warming-induced biome transition under chronic warming[77]. Unlike chronic climate stresses, fires are acute disturbances and thus are less likely to be preceded by reduced resilience[27]. While our results support this expectation in most non-woody ecosystems, reduced resilience was also detected before fires, especially in deciduous forests (Fig. 4c). This pattern could result from fire occurrence being coupled with chronic stress in woody ecosystems, such as low fuel moisture due to long-term climate stress[78]. The long ecological memory and fire–climate coupling in Arctic-boreal ecosystems highlight the potential of leveraging remotely sensed resilience to monitor and predict abrupt vegetation changes. Nonetheless, resilience did not always reduce and did not reduce with consistent lead times and magnitude before all abrupt changes. Possible reasons include that different ecosystems could have varying capacities to operate under low resilience and experienced different perturbations which eventually contributed to vegetation changes. Additionally, remotely sensed LCCs may not necessarily be regime shifts but could result from gradual fractional changes of co-existing vegetation types. Thus, decreased resilience across ecosystems may not indicate the same risk of vegetation loss. Future work is needed to assess the impacts of these factors and quantify the capacity of using reduced resilience to predict vegetation shifts.

Although the estimated resilience changes are robust with respect to model uncertainty, we note that further uncertainty still remains due to challenges in high-latitude optical remote sensing that could undermine data quality, such as low sun angle, cloud cover, snow and standing water[67]. Greenness as an optical property does not capture multiple ecological and biophysical aspects of vegetation states such as signals from mixed canopy layers and species. Thus, the ecosystem-scale resilience of greenness estimated here may differ from the resilience of photosynthetic capacity, biomass, community composition and structure[79]. Nevertheless, opportunities exist in leveraging satellite-detected areas of low resilience to diagnose its implications on reduced growth and productivity. Moreover, the post-disturbance resilience quantified here measures the recovery rate to the new equilibrium states which may be different from the

prechange states (Extended Data Fig. 5). It offers a starting point to address the challenge of monitoring ecosystem recovery at a large scale[79–81], assess discrepancies with the recovery of ecosystem composition and carbon sink[16] and identify ecological and environmental factors that could contribute to bridging the gaps. Doing so will contribute to providing operational indicators of Arctic-boreal ecosystem change and functions[79].

In summary, our results reveal that vegetation resilience mostly increased in tundra ecosystems but significantly decreased in southern boreal forests in northwestern North America, particularly in warmer and drier areas, and further diminished along with LCCs and fires. The declining resilience, including that in greening areas, indicates that impaired ecosystem stability could potentially dampen expected increase of the Arctic-boreal carbon sink strength under future climate. Given the expected increase of climate variability and disturbances, reduced resilience in southern boreal forests implies a higher risk of biome transitions. Our findings motivate further modelling and observational research to better characterize the roles of ecosystem resilience in predicting vegetation shifts and carbon budgets of Arctic-boreal ecosystems.

Methods

The area of interest is the vegetated area within the NASA ABoVE core domain. Vegetated area refers to areas with land-cover type as evergreen forest, deciduous forest, shrubland, herbaceous, sparsely vegetated, barren, fen and bog in 2000[82]. The 3.6 M km^2 region spans over Alaska and northwestern Canada, where the ecosystems are facing rapid climate change and increasing disturbances. Rich datasets on LCC, disturbance and environmental conditions have been developed for the domain, allowing an indepth investigation of vegetation resilience change and its driving factors. We estimated vegetation resilience for each 300 m pixel within the domain from the temporal variation of the EVI with a 16-day interval. Following established studies[26,40–42], we used the negative lag-1 autocorrelation of EVI as a proxy of vegetation resilience. That is, a high autocorrelation indicates low resilience. Here, we considered the temporal variation of EVI to be simultaneously driven by trend, seasonality, climate forcing and autocorrelation. To disentangle autocorrelation from the blended signal, we used a Bayesian time-series model. The model estimated time-varying resilience (negative lag-1 autocorrelation of EVI) for every 16-day interval for each pixel, which was then analysed to (1) quantify the long-term trend of resilience using a simple linear regression; (2) for areas unaffected by LCCs or disturbances, identify critical environmental controls on the sign of resilience trend using random forest classification models[83]; and (3) for areas experiencing LCC or disturbed by fire, investigate resilience change before and after the change/disturbance. Next, we describe the datasets, the Bayesian model setup and the specifics in addressing each of the three objectives.

EVI, land cover, disturbance and environment datasets

To characterize the variation of vegetation state, we collected 250 m, 16-day EVI representing greenness from the MOD13Q1v061 for 2000–2019[48]. Observations affected by snow, ice or cloud according to the quality-control band and EVI values <0.1 were treated as missing data. Areas with >75% missing data among all 16-day time steps were excluded from the analyses. The polar orbit and short revisit time of MODIS provide valid observations more frequently in Arctic-boreal regions, which is essential for effectively detecting the autocorrelation signal. Vegetation state variables used in previous large-scale studies included the NDVI and its derivative and the VOD[26,41,42]. EVI was used here because it incorporates atmospheric corrections and subdues canopy background noises and is less susceptible to saturation in boreal forests than is NDVI[84]. Unlike VOD which requires merging records from multiple instruments to obtain sufficiently long time series, making the estimated resilience unreliable[85], MODIS EVI is consistent across the record.

Land-cover and annual changes were characterized using a 30 m Landsat-based annual land-cover product across the ABoVE core domain from 2000 to 2014[82]. Disturbances were identified from two datasets: (1) Landsat-based annual disturbance agents of fire, insects and logging at a 30 m resolution across the ABoVE core domain from 2000 to 2012[7] and (2) MODIS-based annual fire locations at a 500 m spatial resolution for Alaska and Canada from 2001 to 2019[52]. Because the former underestimated disturbance occurrences at the end of the time frame (2011 and 2012) as its algorithm requires sufficient consecutive observations to detect a disturbance[7], we combined the Landsat-based disturbance maps during 2000–2010 and the MODIS-based fire maps during 2011–2019.

Data on environmental characteristics include climate, ALT, topography, soil moisture and soil nitrogen content. Monthly climate data from 2001 to 2019 at a 4 km resolution were obtained from ClimateNA, a regionally downscaled product from the gridded Climatic Research Unit time-series data v.4.02 (ref. 86). Climate conditions considered here included multiple variables of temperature, humidity, climate dryness, precipitation and snow (Supplementary Table 1). The monthly climate variables were linearly interpolated to the 16-day timestamps consistent with those of EVI. The annual ALT data were from an ~900 m re-analysis product from the Climate Change Initiative (CCI) of the European Space Agency (ESA) v.3.0 (ref. 87). We used elevation data at a 30 m resolution from the advanced spaceborne thermal emission and reflection radiometer digital elevation model v.3 (ref. 88). Slope and aspect were derived from elevation using the Python package RichDEM (v.0.3.4)[89]. Long-term averages of summer soil moisture were obtained from the 25 km ESA CCI product v.07.1 (ref. 90). In addition, we used 250 m soil nitrogen content from the SoilGrids v.2 product, integrated over 0–30 cm depths[91]. All datasets were resampled to a 300 m spatial resolution under the Canadian Albers Equal Area projection using the nearest-neighbour method.

Bayesian DLM for resilience estimation

We used a DLM to estimate the time-varying vegetation resilience (negative lag-1 autocorrelation of EVI) with a 16-day interval for each pixel with Bayesian inference. The model jointly estimates lag-1 autocorrelation and other components including mean and trend, seasonality, climate impact and observational noise which simultaneously affect the observed EVI. Unlike the commonly used moving window approach which is sensitive to the window length of choice and climate variations[42,72], DLM showed robustness in disentangling resilience signals in temperate forests[28]. The autocorrelation of climate and a short- or long-term trend of greenness are unlikely to cause a false signal of resilience change (Supplementary Method 1 and Extended Data Fig. 1).

To build an effective and parsimonious DLM, we needed to determine which climate variables to include for characterizing the impact of climate on EVI. However, the computational cost prohibited us from performing model selection using the Bayesian DLM. Therefore, we first selected the most informative climate variables using multilinear regressions and the Bayesian information criterion (BIC). Specifically, we classified 12 candidate climate variables (Supplementary Table 1) into a temperature group and a moisture group. The former includes the mean, maximum and minimum temperatures, the degree days <0 °C (DD_0) and >5 °C (DD5), the number of frost-free days and the reference evaporation. The latter includes climate moisture deficit (CMD), relative humidity, vapour pressure deficit (VPD), precipitation and precipitation as snow (PAS). Climate conditions at $t-1$ were used to model the EVI at t to allow EVI to exhibit lagged responses to climate[92–94]. We generated 48 combinations by choosing up to one variable from each group and fitted 48 linear models, regressing the EVI at time t with climate and the EVI at time $t-1$ for each pixel. Ranked by BIC, the model that exclusively included mean temperature ranks among the best ten models for 67% of the pixels across the domain (Supplementary Table 2). The mean temperature was therefore consistently used across the domain to characterize the climate impact on EVI variation in DLM, as detailed next.

The DLM model setup was adapted from ref. 28 as follows:

$$y_t = \mathbf{F}_t{}^T \boldsymbol{\theta}_t + \upsilon_t \quad (1)$$

$$\boldsymbol{\theta}_t = G\boldsymbol{\theta}_{t-1} + \mathbf{W}_t \quad (2)$$

where y_t is the observed EVI at each 16-day time step t after removing the long-term mean at a pixel. The model disentangles the temporal variation of y_t into a Gaussian observational noise (υ_t) and three components: the mean and trend component $y_{l,t}$, the seasonality component $y_{s,t}$ and the regression component $y_{r,t}$, giving $y_t = y_{l,t} + y_{s,t} + y_{r,t} + \upsilon_t$. Correspondingly, $\mathbf{F}_t$ (equation (3)) is a vector consisting of known constants and regressors used to aggregate the three components in the state vector $\boldsymbol{\theta}_t$ (equation (4)). Specifically, $\mathbf{F}_{l,t}$ aggregates the mean and trend component $\boldsymbol{\theta}_{l,t}$, where $\theta_{l1,t}$ and $\theta_{l2,t}$ describe the mean of $y_{l,t}$ and its change from $t-1$ to t, respectively, representing the equilibrium state that could adapt to observations to account for shifted equilibrium regime after vegetation changes; $\mathbf{F}_{s,t}$ aggregates the seasonal cycle $\boldsymbol{\theta}_{s,t}$ described by two Fourier components with periods of one year and a half year; and $\mathbf{F}_{r,t}$ includes the EVI (y_{t-1}) and the z-score of mean air temperature (T_{t-1}) at the previous time step, which yields $y_{r,t}$ when multiplied with the regression coefficients $\boldsymbol{\theta}_{r,t} = (\theta_{\mathrm{lag1},t}, \theta_{T(t-1),t})^T$. We were particularly interested in the lag-1 autocorrelation of EVI ($\theta_{\mathrm{lag1},t}$) and used $-\theta_{\mathrm{lag1},t}$ to measure resilience. The state vector $\boldsymbol{\theta}_t$ evolves from $t-1$ to t based on an evolution matrix $G = \mathrm{diag}(G_l, G_s, G_r)$, where the mean and trend (G_l), seasonality (G_s) and regression (G_r) components consist of known constants (equation (5)).

$$\mathbf{F}_t = [\underbrace{1,0}_{\mathbf{F}_{l,t}}, \underbrace{1,0,1,0}_{\mathbf{F}_{s,t}}, \underbrace{y_{t-1}, T_{t-1}}_{\mathbf{F}_{r,t}}]^T \quad (3)$$

$$\boldsymbol{\theta}_t = [\underbrace{\theta_{l1,t}, \theta_{l2,t}}_{\boldsymbol{\theta}_{l,t}}, \underbrace{\theta_{s11,t}, \theta_{s12,t}, \theta_{s21,t}, \theta_{s22,t}}_{\boldsymbol{\theta}_{s,t}}, \underbrace{\theta_{lag1,t}, \theta_{T(t-1),t}}_{\boldsymbol{\theta}_{r,t}}]^T \quad (4)$$

$$G_l = \begin{bmatrix} 1 & 1 \\ 0 & 1 \end{bmatrix}, G_s = \begin{bmatrix} G_{s1} & 0 \\ 0 & G_{s2} \end{bmatrix}, G_{si} = \begin{bmatrix} \cos\omega_i & \sin\omega_i \\ -\sin\omega_i & \cos\omega_i \end{bmatrix}$$
$$\left(i = 1,2; \omega_1 = \frac{\pi}{6}, \omega_2 = \frac{\pi}{3}\right) G_r = \begin{bmatrix} 1 & 0 \\ 0 & 1 \end{bmatrix} \quad (5)$$

We used Bayesian inference to estimate the resilience embedded in $\boldsymbol{\theta}_t$ at each time step. Specifically, $\boldsymbol{\theta}_t$ was assumed to follow a multivariate Gaussian distribution. The same non-informative priors as described in ref. 28 were used for $\boldsymbol{\theta}_{t=0}$ and the noise. At each time step t, the posterior distribution of $\boldsymbol{\theta}_t$, $p(\boldsymbol{\theta}|\, y_1, \ldots, y_{t-1}, y_t)$ was estimated based on the Bayes theorem by combining the prior of $\boldsymbol{\theta}_t$, that is, $p(\boldsymbol{\theta}_t|\, y_1, \ldots, y_{t-1})$, derived from historical observations ($y_1, \ldots, y_{t-1}$) and the likelihood of observing y_t, that is, $p(y_t|\boldsymbol{\theta}_t, y_1, \ldots, y_{t-1})$ (equation (6)). When y_t was missing because of snow, ice, cloud or invalid values, the prior $p(\boldsymbol{\theta}_t|\, y_1, \ldots, y_{t-1})$ was used to estimate $\boldsymbol{\theta}_t$. In this case, due to the stochastic noise $\mathbf{W}_t$, the missing data would increase the variance of $\boldsymbol{\theta}_t$ and thus the uncertainty of the estimated resilience:

$$p(\boldsymbol{\theta}_t|\, y_1, \ldots, y_{t-1}, y_t) \propto p(\boldsymbol{\theta}_t|\, y_1, \ldots, y_{t-1}) p(y_t|\boldsymbol{\theta}_t, y_1, \ldots, y_{t-1}) \quad (6)$$

To estimate the temporal variation of resilience, a moving window approach uses only data within a time length to the target step without accounting for data at earlier times. Likewise, here, we applied a discounting factor δ that reduces the weight of the prior derived from the historical data, allowing the posterior to be updated to the current observation, that is, a forgetting process. Reducing the weight of the prior was achieved by inflating the prior variance of $\boldsymbol{\theta}_t$ by $1/\delta - 1$ from $t-1$ to t (refs. 28,49). Specifically, denoting the variance of $\boldsymbol{\theta}_{t-1}$ as $\mathrm{Var}(\boldsymbol{\theta}_{t-1}|y_1, \ldots, y_{t-1}) = C_{t-1}$. On the basis of equation (2), the prior variance of $\boldsymbol{\theta}_t$ is $\mathrm{Var}(\boldsymbol{\theta}_t|y_1, \ldots, y_{t-1}) = GC_{t-1}G^T + \mathbf{W}_t$, where $\mathbf{W}_t$ is the covariance of the evolution noise. Because $\mathbf{W}_t$ was unknown, it was assumed to be proportional to $GC_{t-1}G^T$, that is, $\mathrm{Var}(\boldsymbol{\theta}_t|y_1, \ldots, y_{t-1}) = GC_{t-1}G^T/\delta$. A discounting factor of 1 represents no forgetting and a δ closer to 1 represents slower forgetting and, expectedly, smaller temporal variability (similar to a larger moving window size). Among the tested range of 0.97–0.99, a discounting factor of 0.98 yielded the highest average model likelihood across the domain, indicating that we have the highest confidence in the estimated resilience and its trend with this factor. Thus, 0.98 was used in the main analyses. Sensitivity analysis using other δ values was shown in Extended Data Fig. 10.

Further mathematical details of the model setup were described in ref. 28. Robustness tests can be found in Supplementary Methods and Extended Data Fig. 1, which demonstrated the effectiveness of DLM in disentangling resilience from blended signals mimicking multiple scenarios of vegetation change using synthetic data.

Calculation of the long-term resilience trend

At each 16-day time step, we tracked the estimated resilience and its uncertainty using the mean and standard deviation of the negative lag-1 autocorrelation of EVI from the posterior distribution of $\boldsymbol{\theta}_t$. Because non-informative priors were used, the model required a spin-up period before enough historical data were accumulated to constrain the uncertainty of resilience estimates (Extended Data Fig. 2). Thus, the resilience estimates within the first 3 years, which typically have large uncertainty, were excluded from the following analyses. The trend of the 16-day posterior mean resilience for each pixel was calculated using the 391 resilience estimates (23 values per year times 17 years, from 2003 to 2019) based on a simple linear regression. We further compared resilience trends in greening and browning areas, defined as pixels showing significant ($\alpha = 0.05$) linear trends in summer EVI from 2000 to 2019. Summer EVI was calculated as the average of values for June, July and August. Trend analyses were conducted in Python using the package statsmodels (v.0.12.2).

To measure the uncertainty in the estimated resilience trend propagated from the uncertainty in estimated resilience, instead of using the posterior mean, we randomly sampled 100 resilience values from the posterior distribution at each time step. The samples yielded 100 sets of resilience trends. The 5th percentile and the 95th percentile of the 100 resilience trends exhibited similar spatial patterns to those using the posterior mean resilience: Arctic tundra and boreal forest showed consistently divergent trends (Extended Data Fig. 9). The similar spatial patterns indicated that the spatial pattern of resilience change using the posterior mean, as presented in the main text, is robust.

Random forests for identifying critical environmental controls

To evaluate what environmental conditions contribute to a high likelihood of resilience reduction, we built a random forest classification model[83] to predict the sign of the resilience trend across space, using factors described in the 'EVI, land cover, disturbance and environment datasets' section. We focused only on areas without LCCs or recorded disturbances to diagnose the influence of environmental conditions on transient resilience change. The environmental conditions included long-term averages of summer mean temperature, annual PAS, summer mean VPD, summer mean CMD, summer mean soil moisture, annual maximum permafrost extent, annual maximum ALT and time-invariant land-cover type, elevation, slope and aspect. Additionally, we included the standard deviation and the trend of summer temperature, as well as the trend of summer EVI, to capture the effect of temporal variation. Among the total 16 variables considered, we identified highly correlated ($r > 0.75$) pairs and removed one variable in each pair, retaining the variables that were important in explaining EVI dynamics as described above. The resulting 14 variables were used as predictors in the random forest model. We focused on the 31.0 M pixels without

recorded LCCs and disturbances, of which nearly 28.4 M pixels showed significant resilience trends. To reduce the computational load of the random forest model, we randomly sampled 100 sets from those 28.4 M pixels, with each set consisting of 56.7 K pixels. Each set included an equal number of pixels with increasing and decreasing resilience to balance the sample size for each category. We randomly partitioned each sample set into the training (75%) and testing (25%) subsets and optimized the number of variables used at each tree node to achieve the highest out-of-bag classification accuracy on the training subset. The resulting optimal random forest model was used to evaluate the classification accuracy on the testing subset and diagnose the impact of each environmental variable. The relative importance of each variable was ranked by the mean decrease in accuracy. To understand the impact of each environmental variable on the resilience trend, we calculated the partial dependence of the classification probability with respect to a range of values for each variable while holding other variables at their mean values. We repeated the above analyses for the 100 sets to quantify the uncertainty (95% confidence interval) associated with the selection of samples. The random forest analyses were conducted in R using the packages of randomForest (v.4.7-1.1)[95], caret (v.6.0-92)[96] and pdp (v.0.8.0)[97].

Resilience variation before and after LCCs or fire disturbances

To investigate resilience trajectories before and after abrupt changes, we analysed pixels that experienced two types of abrupt changes: LCC without recorded disturbance (that is, climate-driven LCC) and fire disturbance. We only focused on pixels with a single LCC event and/or disturbance event. For climate-driven LCC, we focused on three types of vegetation loss and four types of vegetation gain following ref. 11. Evergreen (deciduous) forest loss was defined as transitions from evergreen (deciduous) forest to shrublands or any non-woody land cover. Evergreen (deciduous) forest gain was defined as transitions from deciduous (evergreen) forest, shrubland or non-woody land cover to evergreen (deciduous) forest. Shrub loss (gain) was defined as transitions to (from) any non-woody land cover. Herbaceous gain was defined as transitions to herbaceous land from sparsely vegetated, barren, fen, bog, shallows or water. Fire-disturbed areas were identified on the basis of products from refs. 7,52. We noted that these two products may omit small fires. Nonetheless, locations with recorded fires still provided a sufficient sample size to diagnose resilience variation. For the same reason, the LCC may not be exclusively driven by climate but could also include changes driven by small disturbances that are omitted in the disturbance products[7,52].

We analysed resilience change before and after LCC and fires at an annual scale, specifically focusing on resilience during the summer, defined as the average of the 16-day resilience values for June, July and August. Between 5 years before and 5 years after the abrupt change, we compared the summer resilience of the target pixel to a baseline. The baseline was determined using two approaches. The first was a temporal baseline, calculated as the averaged resilience from 2003 up to 5 years before the abrupt change for the same pixel. The second was a spatial baseline, calculated as the averaged resilience across control pixels in the year of the abrupt change, adjusted for the spatial differences in initial resilience conditions. The control pixels were selected as nearby (<9 km) pixels with the same initial land cover in 2003 and a similar environment to the target pixel but without any abrupt changes. The environment was considered similar if the Euclidean distance in the space for the *z*-scores of summer mean temperature, ALT and elevation—the top three factors explaining the resilience trend (Fig. 3a)—between the target and candidate control pixels was less than the 10th percentile. Specifically, the impact of climate-driven LCC or fire on the resilience in pixel *j* was calculated as follows, with respect to the temporal baseline (equation (7)) and the spatial baseline (equation (8)), respectively.

$$\Delta R_j^t = R_{j,y} - \bar{R}_{j,\mathrm{init}}^t \tag{7}$$

$$\Delta R_j^s = \left(R_{j,y} - \bar{R}_{\mathrm{ctrl},y}^s\right) - \left(R_{j,2003} - \bar{R}_{\mathrm{ctrl},2003}^s\right) \tag{8}$$

where ΔR_j^t is resilience change with respect to the temporal baseline, $R_{j,y}$ is the summer resilience of pixel j in year y and $\bar{R}_{j,\mathrm{init}}^t$ is the average summer resilience from 2003 up to 5 years before the abrupt change; ΔR_j^s is resilience change with respect to the spatial baseline, $\bar{R}_{\mathrm{ctrl},y}^s$ is the average summer resilience across control pixels in year y, $R_{j,2003}$ is the summer resilience of pixel j in 2003 and $\bar{R}_{\mathrm{ctrl},2003}^s$ is the average summer resilience across control pixels in 2003. The spatial and temporal baselines provided controls of resilience unaffected by LCC or fire under different assumptions, thereby allowing us to examine resilience variations impacted by the corresponding abrupt changes. We sampled 10 K pixels for each of the seven LCC types from 2.6 M pixels with LCC and 10 K pixels for each of the five prefire land-cover types from 2.9 M pixels with fire. The resilience variations were grouped by LCC types for LCC pixels and by the prefire land-cover type for fire-disturbed pixels. At each target year (for example, 5 years before LCC), the fraction of pixels with negative ΔR in each group was calculated to quantify the likelihood of decreasing resilience associated with LCC or fire. We repeated the sampling with replacement 100 times to quantify uncertainty.

To account for different ecosystem dynamics after LCC and fires, we also set up an alternative version of the Bayesian DLM with intervention at the time of LCC or fire. This was achieved by inflating the covariance matrix of the prior (C_{t-1} in the Methods) for the state variables by a factor of 2, as recommended by ref. 49. Inflating the covariance matrix of the prior distribution is equivalent to reducing the weight of historical information on the inference at the current time step, of which the imprint is carried afterwards. The posterior estimates of resilience and other state variables thus rely more on new observations after the intervention. Compared to the default version without intervention, this alternative model version relies more heavily on and adapts more quickly to new observations shortly after the change. However, the alternative model is more susceptible to observational noise and bias due to the limited number of observations shortly after disturbance. Thus, the Bayesian model with intervention is more representative of severe disturbances which reset the ecosystem dynamics while yielding excessive estimates of resilience uncertainty. In contrast, the model without intervention is better suited for climate-driven LCC and provides a more conservative estimate of uncertainty. We analysed the resilience trajectories in all pixels that experienced LCC and fires using two versions of the Bayesian DLM with and without intervention. This approach helped assess the uncertainty and robustness of resilience trajectories following these changes.

Reporting summary

Further information on research design is available in the Nature Portfolio Reporting Summary linked to this article.

Data availability

The annual resilience maps produced in this study are archived and freely available at the NASA ORNL Active Archive Center (DAAC) (https://doi.org/10.3334/ORNLDAAC/2374)[98]. All datasets used in this study are publicly available. The MODIS EVI dataset is available at https://lpdaac.usgs.gov/products/mod13q1v061/. The annual land-cover product is available at https://daac.ornl.gov/ABOVE/guides/Annual_Landcover_ABoVE.html. The climate conditions and the application to downscale (ClimateNA) are available at https://climatena.ca/. The disturbances datasets are available at https://daac.ornl.gov/ABOVE/guides/ABoVE_ForestDisturbance_Agents.html and https://daac.ornl.gov/ABOVE/guides/Burned_Area_Depth_AK_CA.html.

ALT data are available at https://catalogue.ceda.ac.uk/uuid/67a3f8c8dc914ef99f7f08eb0d997e23. The ASTER DEM is available at https://lpdaac.usgs.gov/products/astgtmv003/. The soil moisture data are from https://catalogue.ceda.ac.uk/uuid/43d73291472444e6b9c2d2420dbad7d6. The soil nitrogen data are from https://www.isric.org/explore/soilgrids.

Code availability

Codes and data for the Bayesian dynamic linear model, the random forest model and the main figures are available via Zenodo at https://doi.org/10.5281/zenodo.10719618 (ref. 99).

References

1. Rantanen, M. et al. The Arctic has warmed nearly four times faster than the globe since 1979. *Commun. Earth Environ.* **3**, 168 (2022).
2. IPCC *Climate Change 2021: The Physical Science Basis* (eds Masson-Delmotte, V. et al.) (Cambridge Univ. Press, 2021).
3. Myneni, R. B., Keeling, C. D., Tucker, C. J., Asrar, G. & Nemani, R. R. Increased plant growth in the northern high latitudes from 1981 to 1991. *Nature* **386**, 698–702 (1997).
4. Pan, Y. et al. A large and persistent carbon sink in the world's forests. *Science* **333**, 988–993 (2011).
5. Epstein, H. E. et al. Dynamics of aboveground phytomass of the circumpolar Arctic tundra during the past three decades. *Environ. Res. Lett.* **7**, 015506 (2012).
6. Piao, S. et al. Characteristics, drivers and feedbacks of global greening. *Nat. Rev. Earth Environ.* **1**, 14–27 (2019).
7. Zhang, Y. et al. Mapping causal agents of disturbance in boreal and arctic ecosystems of North America using time series of Landsat data. *Remote Sens. Environ.* **272**, 112935 (2022).
8. Foster, A. C. et al. Disturbances in North American boreal forest and Arctic tundra: impacts, interactions, and responses. *Environ. Res. Lett.* **17**, 113001 (2022).
9. Liu, Q. et al. Drought-induced increase in tree mortality and corresponding decrease in the carbon sink capacity of Canada's boreal forests from 1970 to 2020. *Glob. Change Biol.* **29**, 2274–2285 (2023).
10. Berner, L. T. et al. Summer warming explains widespread but not uniform greening in the Arctic tundra biome. *Nat. Commun.* **11**, 4621 (2020).
11. Wang, J. A. et al. Extensive land cover change across Arctic-Boreal Northwestern North America from disturbance and climate forcing. *Glob. Change Biol.* **26**, 807–822 (2020).
12. Berner, L. T. & Goetz, S. J. Satellite observations document trends consistent with a boreal forest biome shift. *Glob. Change Biol.* **28**, 3275–3292 (2022).
13. Ju, J. & Masek, J. G. The vegetation greenness trend in Canada and US Alaska from 1984–2012 Landsat data. *Remote Sens. Environ.* **176**, 1–16 (2016).
14. Mekonnen, Z. A. et al. Arctic tundra shrubification: a review of mechanisms and impacts on ecosystem carbon balance. *Environ. Res. Lett.* **16**, 053001 (2021).
15. Michaelian, M., Hogg, E. H., Hall, R. J. & Arsenault, E. Massive mortality of aspen following severe drought along the southern edge of the Canadian boreal forest. *Glob. Change Biol.* **17**, 2084–2094 (2011).
16. Baltzer, J. L. et al. Increasing fire and the decline of fire adapted black spruce in the boreal forest. *Proc. Natl Acad. Sci. USA* **118**, e2024872118 (2021).
17. Wang, J. A., Baccini, A., Farina, M., Randerson, J. T. & Friedl, M. A. Disturbance suppresses the aboveground carbon sink in North American boreal forests. *Nat. Clim. Change* **11**, 435–441 (2021).
18. Mack, M. C. et al. Carbon loss from boreal forest wildfires offset by increased dominance of deciduous trees. *Science* **372**, 280–283 (2021).
19. Braghiere, R. K. et al. Tipping point in North American Arctic-boreal carbon sink persists in new generation Earth system models despite reduced uncertainty. *Environ. Res. Lett.* **18**, 025008 (2023).
20. Randerson, J. T. et al. The impact of boreal forest fire on climate warming. *Science* **314**, 1130–1132 (2006).
21. Lafleur, P. M. & Humphreys, E. R. Tundra shrub effects on growing season energy and carbon dioxide exchange. *Environ. Res. Lett.* **13**, 055001 (2018).
22. Ito, A. et al. Pronounced and unavoidable impacts of low-end global warming on northern high-latitude land ecosystems. *Environ. Res. Lett.* **15**, 044006 (2020).
23. Brovkin, V. et al. Past abrupt changes, tipping points and cascading impacts in the Earth system. *Nat. Geosci.* **14**, 550–558 (2021).
24. Reyer, C. P. O. et al. Forest resilience and tipping points at different spatio-temporal scales: approaches and challenges. *J. Ecol.* **103**, 5–15 (2015).
25. Scheffer, M., Carpenter, S. R., Dakos, V. & van Nes, E. H. Generic indicators of ecological resilience: inferring the chance of a critical transition. *Annu. Rev. Ecol. Evol. Syst.* **46**, 145–167 (2015).
26. Boulton, C. A., Lenton, T. M. & Boers, N. Pronounced loss of Amazon rainforest resilience since the early 2000s. *Nat. Clim. Change* **12**, 271–278 (2022).
27. Dakos, V. & Kéfi, S. Ecological resilience: what to measure and how. *Environ. Res. Lett.* **17**, 043003 (2022).
28. Liu, Y., Kumar, M., Katul, G. G. & Porporato, A. Reduced resilience as an early warning signal of forest mortality. *Nat. Clim. Change* **9**, 880–885 (2019).
29. Tai, X., Trugman, A. T. & Anderegg, W. R. L. Linking remotely sensed ecosystem resilience with forest mortality across the continental United States. *Glob. Change Biol.* **29**, 1096–1105 (2023).
30. Cailleret, M. et al. A synthesis of radial growth patterns preceding tree mortality. *Glob. Change Biol.* **23**, 1675–1690 (2017).
31. Wu, D. et al. Reduced ecosystem resilience quantifies fine-scale heterogeneity in tropical forest mortality responses to drought. *Glob. Change Biol.* **28**, 2081–2094 (2022).
32. Johnstone, J. F. et al. Decadal observations of tree regeneration following fire in boreal forests. *Can. J. For. Res.* **34**, 267–273 (2004).
33. Xu, C. et al. Long-term forest resilience to climate change indicated by mortality, regeneration, and growth in semiarid southern Siberia. *Glob. Change Biol.* **23**, 2370–2382 (2017).
34. Whitman, E., Parisien, M.-A., Thompson, D. K. & Flannigan, M. D. Short-interval wildfire and drought overwhelm boreal forest resilience. *Sci. Rep.* **9**, 18796 (2019).
35. Isaac-Renton, M. et al. Northern forest tree populations are physiologically maladapted to drought. *Nat. Commun.* **9**, 5254 (2018).
36. DeSoto, L. et al. Low growth resilience to drought is related to future mortality risk in trees. *Nat. Commun.* **11**, 545 (2020).
37. Camarero, J. J., Gazol, A., Sangüesa-Barreda, G., Oliva, J. & Vicente-Serrano, S. M. To die or not to die: early warnings of tree dieback in response to a severe drought. *J. Ecol.* **103**, 44–57 (2015).
38. Harris, R. M. B. et al. Biological responses to the press and pulse of climate trends and extreme events. *Nat. Clim. Change* **8**, 579–587 (2018).
39. Ratajczak, Z. et al. The interactive effects of press/pulse intensity and duration on regime shifts at multiple scales. *Ecol. Monogr.* **87**, 198–218 (2017).
40. Scheffer, M. et al. Early-warning signals for critical transitions. *Nature* **461**, 53–59 (2009).

41. Forzieri, G., Dakos, V., McDowell, N. G., Ramdane, A. & Cescatti, A. Emerging signals of declining forest resilience under climate change. *Nature* **608**, 534–539 (2022).
42. Smith, T., Traxl, D. & Boers, N. Empirical evidence for recent global shifts in vegetation resilience. *Nat. Clim. Change* **12**, 477–484 (2022).
43. McDowell, N. G., Sapes, G. & Pivovaroff, A. Mechanisms of woody-plant mortality under rising drought, CO_2 and vapour pressure deficit. *Nat. Rev. Earth Environ.* **3**, 294–308 (2022).
44. Verbesselt, J. et al. Remotely sensed resilience of tropical forests. *Nat. Clim. Change* **6**, 1028–1031 (2016).
45. Dakos, V. et al. Methods for detecting early warnings of critical transitions in time series illustrated using simulated ecological data. *PLoS ONE* **7**, e41010 (2012).
46. Nazarimehr, F., Jafari, S., Perc, M. & Sprott, J. C. Critical slowing down indicators. *EPL* **132**, 18001 (2020).
47. Dakos, V., Carpenter, S. R., van Nes, E. H. & Scheffer, M. Resilience indicators: prospects and limitations for early warnings of regime shifts. *Philos. Trans. R. Soc. Lond. B* **370**, 20130263 (2015).
48. Didan, K. MOD13Q1 v061: MODIS/Terra Vegetation Indices 16-Day L3 Global 250 m SIN Grid. *LP DACC* https://doi.org/10.5067/MODIS/MOD13Q1.061 (2021).
49. Prado, R. & West, M. *Time Series: Modeling, Computation, and Inference* (Chapman and Hall, 2010).
50. Du, E. et al. Global patterns of terrestrial nitrogen and phosphorus limitation. *Nat. Geosci.* **13**, 221–226 (2020).
51. Mekonnen, Z. A., Riley, W. J. & Grant, R. F. Accelerated nutrient cycling and increased light competition will lead to 21st century shrub expansion in North American Arctic tundra. *J. Geophys. Res. Biogeosci.* **123**, 1683–1701 (2018).
52. Potter, S. et al. ABoVE: Burned Area, Depth, and Combustion for Alaska and Canada, 2001-2019. *ORNL DAAC* https://doi.org/10.3334/ORNLDAAC/2063 (2022).
53. Keenan, T. F. & Riley, W. J. Greening of the land surface in the world's cold regions consistent with recent warming. *Nat. Clim. Change* **8**, 825–828 (2018).
54. Klupar, I., Rocha, A. V. & Rastetter, E. B. Alleviation of nutrient co-limitation induces regime shifts in post-fire community composition and productivity in Arctic tundra. *Glob. Change Biol.* **27**, 3324–3335 (2021).
55. Schore, A. I. G., Fraterrigo, J. M., Salmon, V. G., Yang, D. & Lara, M. J. Nitrogen fixing shrubs advance the pace of tall-shrub expansion in low-Arctic tundra. *Commun. Earth Environ.* **4**, 421 (2023).
56. Myers-Smith, I. H. et al. Shrub expansion in tundra ecosystems: dynamics, impacts and research priorities. *Environ. Res. Lett.* **6**, 045509 (2011).
57. Smith, T. & Boers, N. Reliability of vegetation resilience estimates depends on biomass density. *Nat. Ecol. Evol.* **7**, 1799–1808 (2023).
58. Li, W. et al. Reassessment of growth-climate relations indicates the potential for decline across Eurasian boreal larch forests. *Nat. Commun.* **14**, 3358 (2023).
59. Rotbarth, R. et al. Northern expansion is not compensating for southern declines in North American boreal forests. *Nat. Commun.* **14**, 3373 (2023).
60. Ma, Z. et al. Regional drought-induced reduction in the biomass carbon sink of Canada's boreal forests. *Proc. Natl Acad. Sci. USA* **109**, 2423–2427 (2012).
61. Yang, J., Zhang, Q., Song, W., Zhang, X. & Wang, X. Radial growth of trees rather than shrubs in boreal forests is inhibited by drought. *Front. Plant Sci.* **13**, 912916 (2022).
62. Ogden, E. L., Cumming, S. G., Smith, S. L., Turetsky, M. R. & Baltzer, J. L. Permafrost thaw induces short-term increase in vegetation productivity in northwestern Canada. *Glob. Change Biol.* **29**, 5352–5366 (2023).
63. Watts, J. D. et al. Carbon uptake in Eurasian boreal forests dominates the high-latitude net ecosystem carbon budget. *Glob. Change Biol.* **29**, 1870–1889 (2023).
64. Wulder, M. A., Hermosilla, T., White, J. C. & Coops, N. C. Biomass status and dynamics over Canada's forests: disentangling disturbed area from associated aboveground biomass consequences. *Environ. Res. Lett.* **15**, 094093 (2020).
65. Anderegg, W. R. L. et al. Hydraulic diversity of forests regulates ecosystem resilience during drought. *Nature* **561**, 538–541 (2018).
66. Wang, J. A. & Friedl, M. A. The role of land cover change in Arctic-boreal greening and browning trends. *Environ. Res. Lett.* **14**, 125007 (2019).
67. Myers-Smith, I. H. et al. Complexity revealed in the greening of the Arctic. *Nat. Clim. Change* **10**, 106–117 (2020).
68. Wang, Z. et al. Vegetation resilience does not increase consistently with greening in China's loess plateau. *Commun. Earth Environ.* **4**, 336 (2023).
69. Jump, A. S. et al. Structural overshoot of tree growth with climate variability and the global spectrum of drought-induced forest dieback. *Glob. Change Biol.* **23**, 3742–3757 (2017).
70. Zhang, Y., Keenan, T. F. & Zhou, S. Exacerbated drought impacts on global ecosystems due to structural overshoot. *Nat. Ecol. Evol.* **5**, 1490–1498 (2021).
71. Scheffer, M. et al. Thresholds for boreal biome transitions. *Proc. Natl Acad. Sci. USA* **109**, 21384–21389 (2012).
72. Rogers, B. M. et al. Detecting early warning signals of tree mortality in boreal North America using multiscale satellite data. *Glob. Change Biol.* **24**, 2284–2304 (2018).
73. Itter, M. S. et al. Boreal tree growth exhibits decadal-scale ecological memory to drought and insect defoliation, but no negative response to their interaction. *J. Ecol.* **107**, 1288–1301 (2019).
74. Buermann, W. et al. Widespread seasonal compensation effects of spring warming on northern plant productivity. *Nature* **562**, 110–114 (2018).
75. Li, Y. et al. Widespread spring phenology effects on drought recovery of Northern Hemisphere ecosystems. *Nat. Clim. Change* **13**, 182–188 (2023).
76. Rao, M. P. et al. Approaching a thermal tipping point in the Eurasian boreal forest at its southern margin. *Commun. Earth Environ.* **4**, 247 (2023).
77. Reich, P. B. et al. Even modest climate change may lead to major transitions in boreal forests. *Nature* **608**, 540–545 (2022).
78. Walker, X. J. et al. Fuel availability not fire weather controls boreal wildfire severity and carbon emissions. *Nat. Clim. Change* **10**, 1130–1136 (2020).
79. Seidl, R. & Turner, M. G. Post-disturbance reorganization of forest ecosystems in a changing world. *Proc. Natl Acad. Sci. USA* **119**, e2202190119 (2022).
80. McDowell, N. G. et al. Pervasive shifts in forest dynamics in a changing world. *Science* **368**, eaaz9463 (2020).
81. Hanbury-Brown, A. R., Ward, R. E. & Kueppers, L. M. Forest regeneration within Earth system models: current process representations and ways forward. *New Phytol.* **235**, 20–40 (2022).
82. Wang, J. A. et al. ABoVE: Landsat-derived Annual Dominant Land Cover Across ABoVE Core Domain, 1984-2014. *ORNL DACC* https://doi.org/10.3334/ORNLDAAC/1691 (2019).
83. Breiman, L. Random forests. *Mach. Learn.* **45**, 5–32 (2001).
84. Jiang, Z., Huete, A. R., Didan, K. & Miura, T. Development of a two-band enhanced vegetation index without a blue band. *Remote Sens. Environ.* **112**, 3833–3845 (2008).
85. Smith, T. et al. Reliability of resilience estimation based on multi-instrument time series. *Earth Syst. Dynam.* **14**, 173–183 (2023).

86. Wang, T., Hamann, A., Spittlehouse, D. & Carroll, C. Locally downscaled and spatially customizable climate data for historical and future periods for North America. *PLoS ONE* **11**, e0156720 (2016).
87. Obu, J. et al. ESA Permafrost Climate Change Initiative (Permafrost_cci): Permafrost Active Layer Thickness for the Northern Hemisphere, v3.0. *NERC EDS Centre for Environmental Data Analysis* https://doi.org/10.5285/67a3f8c8dc914ef99f7f08eb0d997e23 (2021).
88. ASTER Global Digital Elevation Model V003. *NASA* https://doi.org/10.5067/ASTER/ASTGTM.003 (2019).
89. Barnes, R. RichDEM: terrain analysis software. *GitHub* http://github.com/r-barnes/richdem (2016).
90. Dorigo, W. et al. ESA Soil Moisture Climate Change Initiative (Soil_Moisture_cci): Ancillary Data Used for the ACTIVE, PASSIVE and COMBINED Products, Version 07.1. *NERC EDS Centre for Environmental Data Analysis* https://doi.org/10.5285/ea3eb0714dc6402b905fe9f7ee50dbbc (2023).
91. Poggio, L. et al. SoilGrids 2.0: producing soil information for the globe with quantified spatial uncertainty. *Soil* **7**, 217–240 (2021).
92. Wu, D. et al. Time-lag effects of global vegetation responses to climate change. *Glob. Change Biol.* **21**, 3520–3531 (2015).
93. Jiao, W. et al. Observed increasing water constraint on vegetation growth over the last three decades. *Nat. Commun.* **12**, 3777 (2021).
94. Wen, Y. et al. Cumulative effects of climatic factors on terrestrial vegetation growth. *J. Geophys. Res. Biogeosci.* **124**, 789–806 (2019).
95. Liaw, A. & Wiener, M. Classification and regression by randomForest. *R News* **2**, 18–22 (2022).
96. Kuhn, M. Building predictive models in R using the caret package. *J. Stat. Softw.* **28**, 1–26 (2008).
97. Greenwell, B. M. pdp: an R package for constructing partial dependence plots. *R J.* **9**, 421–436 (2017).
98. Zhang, Y. & Liu, Y. MODIS-derived Annual Vegetation Resilience, 2000-2019. *ORNL DACC* https://doi.org/10.3334/ORNLDAAC/2374 (2024).
99. Zhang, Y. et al. Codes and data to assess Arctic-boreal Northwestern North America vegetation resilience. *Zenodo* https://doi.org/10.5281/zenodo.10719618 (2024).

Acknowledgements

This study was part of the Arctic-Boreal Vulnerability Experiment supported by NASA Terrestrial Ecology Program grants 80NSSC22K1249 (Y.Z. and Y.L.), 80NSSC22K1247 (S.J.G. and L.T.B.) and 80NSSC23K0140 (J.A.W.). Computing resources were provided by the Ohio Supercomputer Center.

Author contributions

Y.L. conceived the study. Y. Z. and Y.L. designed the analyses. Y.Z. prepared data and performed the analysis with inputs from all authors. Y.Z. and Y.L. led the manuscript writing. All authors contributed to interpreting the results and editing the manuscript.

Competing interests

The authors declare no competing interests.

Additional information

Extended data is available for this paper at https://doi.org/10.1038/s41559-024-02551-0.

Supplementary information The online version contains supplementary material available at https://doi.org/10.1038/s41559-024-02551-0.

Correspondence and requests for materials should be addressed to Yanlan Liu.

Peer review information *Nature Ecology & Evolution* thanks Ronny Rotbarth and the other, anonymous, reviewer(s) for their contribution to the peer review of this work. Peer reviewer reports are available.

https://doi.org/10.1038/s41559-024-02551-0

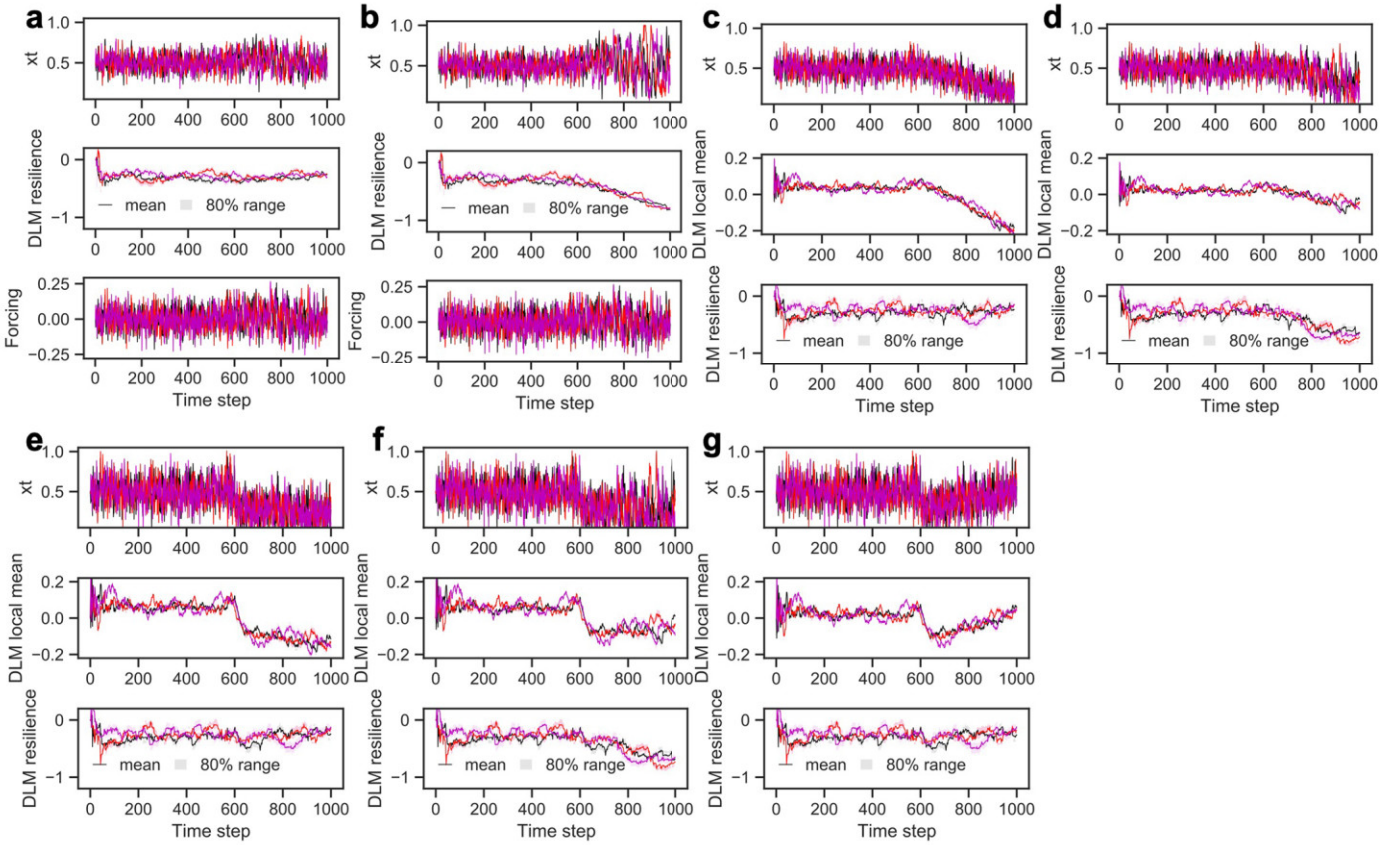

Extended Data Fig. 1 | Theoretical experiments showing the detected resilience change is unlikely a false signal due to autocorrelated climate, EVI trend, abrupt drop, or localized postfire recovery. The three colours represent synthetic series generated using different random noises. The detailed experimental setup is described in the Supplementary Information. **(a)** High climate autocorrelation after the time step 600 does not cause a false signal of low vegetation resilience estimated by DLM. **(b)** Prescribed resilience decline can be captured by estimates of DLM. **(c)** A browning trend does not raise a false signal of decreasing resilience but is captured by the local mean component in DLM. **(d)** Reduced resilience blended with a browning trend can be disentangled using DLM. **(e)** Abrupt EVI drop, for example, after forest loss or fire, does not cause a false signal of decreasing resilience. Rather, the shifted equilibrium state is captured by the local mean component in DLM. **(f)** Reduced resilience blended with abrupt EVI drop can be disentangled using DLM. **(g)** Abrupt EVI drop followed by a localized recovery trend, representing postfire recovery, does not cause a false signal of decreasing vegetation resilience but is captured by the local mean component in DLM. In the DLM resilience panels from **(a)** to **(g)**, the lines denote the mean, and the shaded bands denote the mid-80th percentile of the uncertainty range of the estimated resilience.

https://doi.org/10.1038/s41559-024-02551-0

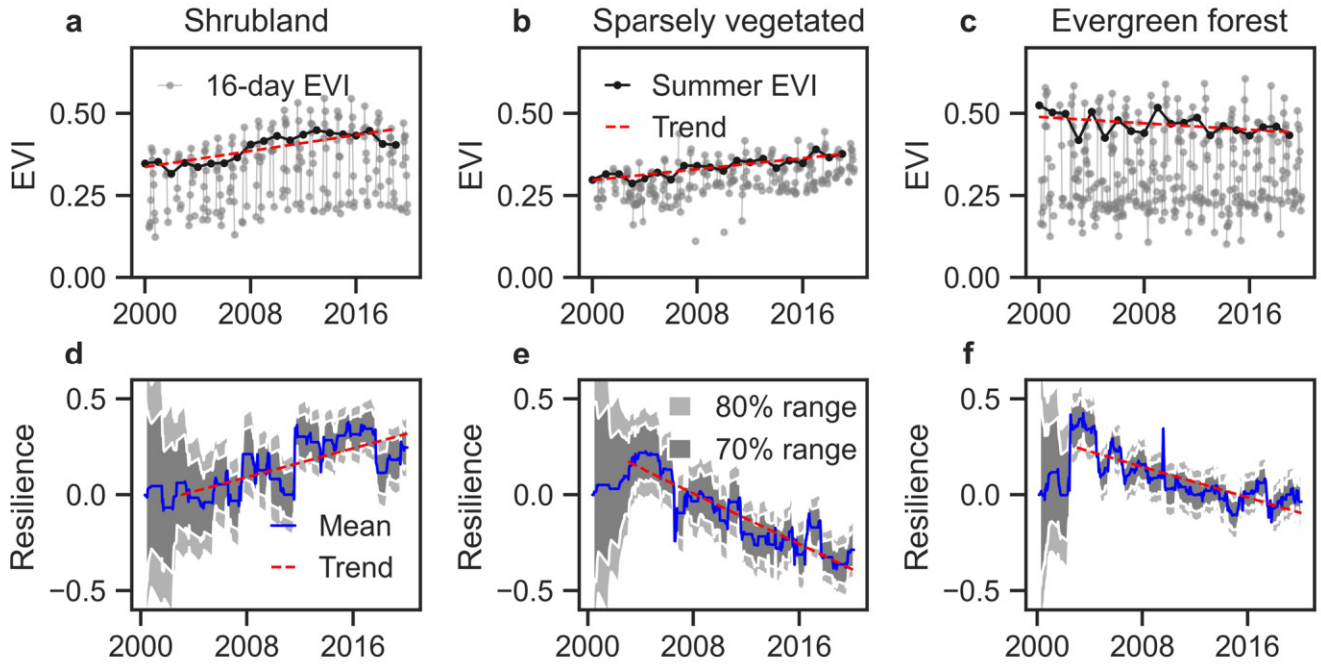

Extended Data Fig. 2 | Three example time series of greenness and vegetation resilience. a-c, The temporal variation of Enhanced Vegetation Index (EVI) in a greening shrubland pixel in southwestern Northwest Territories (62.2°N, 124.1°W) (**a**), a greening sparsely vegetated pixel in southwestern Alaska (59.7°N, 156.0°W) (**b**), and a browning evergreen forest pixel in northeastern British Columbia (58.5°N, 123.3°W) (**c**). The gray and black dotted lines are 16-day EVI and summer (June, July, August) averages, respectively; the red dashed lines show the linear trends. **d-f**, The temporal variation of vegetation resilience (negative lag-1 autocorrelation of 16-day EVI shown in **a-c**). The blue lines denote the mean, and the light and dark gray bands denote the mid-80th and mid-70th percentile of the uncertainty ranges of the estimated resilience, respectively. The red dashed lines are the linear trends of the mean from 2003 onward after discarding the three-year spin-up period. The x-axis labels represent January 1st of each year.

https://doi.org/10.1038/s41559-024-02551-0

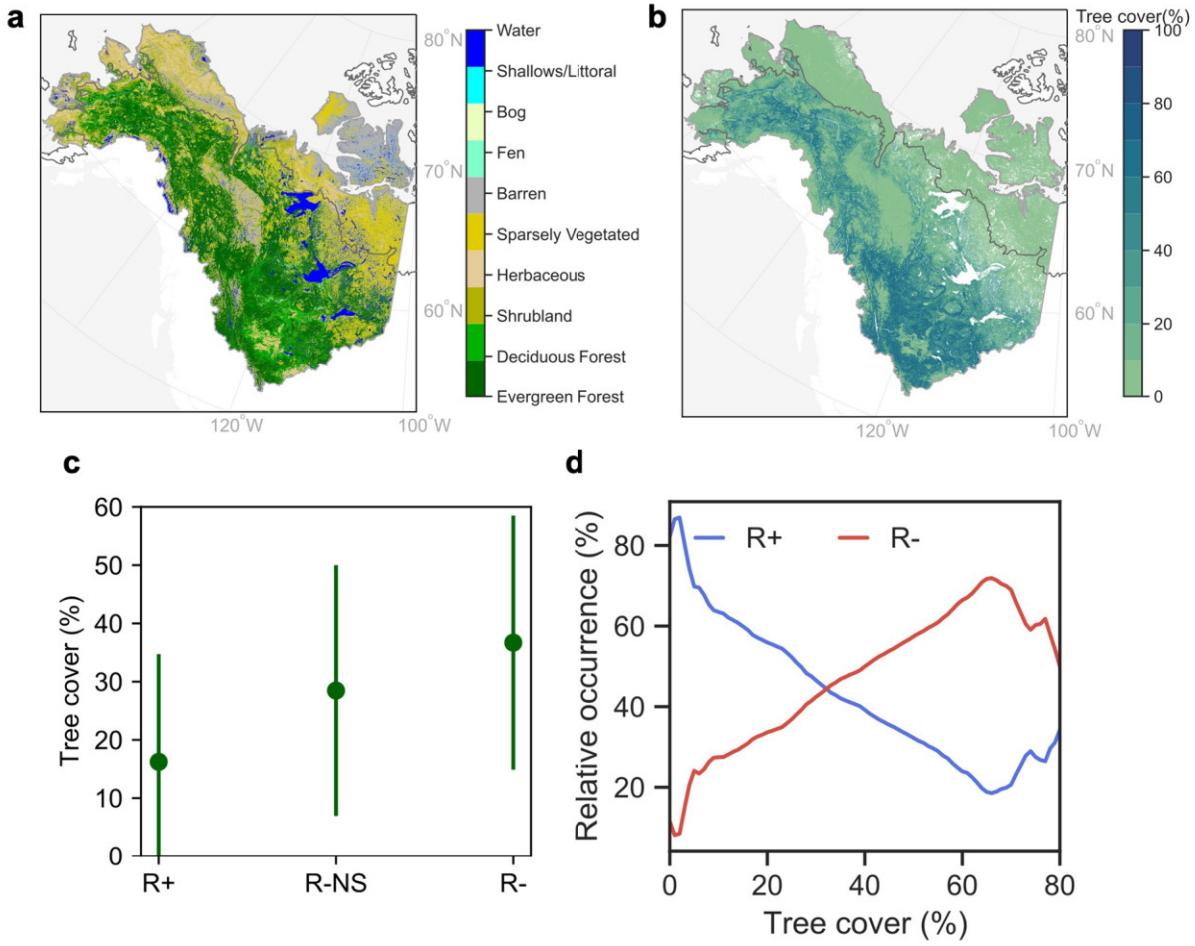

Extended Data Fig. 3 | Boreal forests with high tree cover experienced extensive resilience declines. (a) Land cover across the ABoVE core domain in 2000. **(b)** Tree cover fraction across the ABoVE core domain in 2003 from MODIS/Terra Vegetation Continuous Fields Yearly L3 Global 250 m SIN Grid (MOD44B v006). The year 2003 instead of 2000 is used for better data quality as MODIS/Terra began broadcasting data in April 2000. **(c)** Tree cover across pixels where vegetation resilience significantly increased (R +), decreased (R-), or did not show a significant trend (R-NS) during 2000–2019. The green dots indicate mean values, and the error bars indicate standard deviations of tree cover across pixels showing R+ (n = 22,090,216), R-NS (n = 3,469,461), and R- (n = 14,079,533). **(d)** The relative frequency of reduced and enhanced resilience across pixels with tree cover binned at 1% increments, with blue and red lines showing R+ and R-, respectively.

https://doi.org/10.1038/s41559-024-02551-0

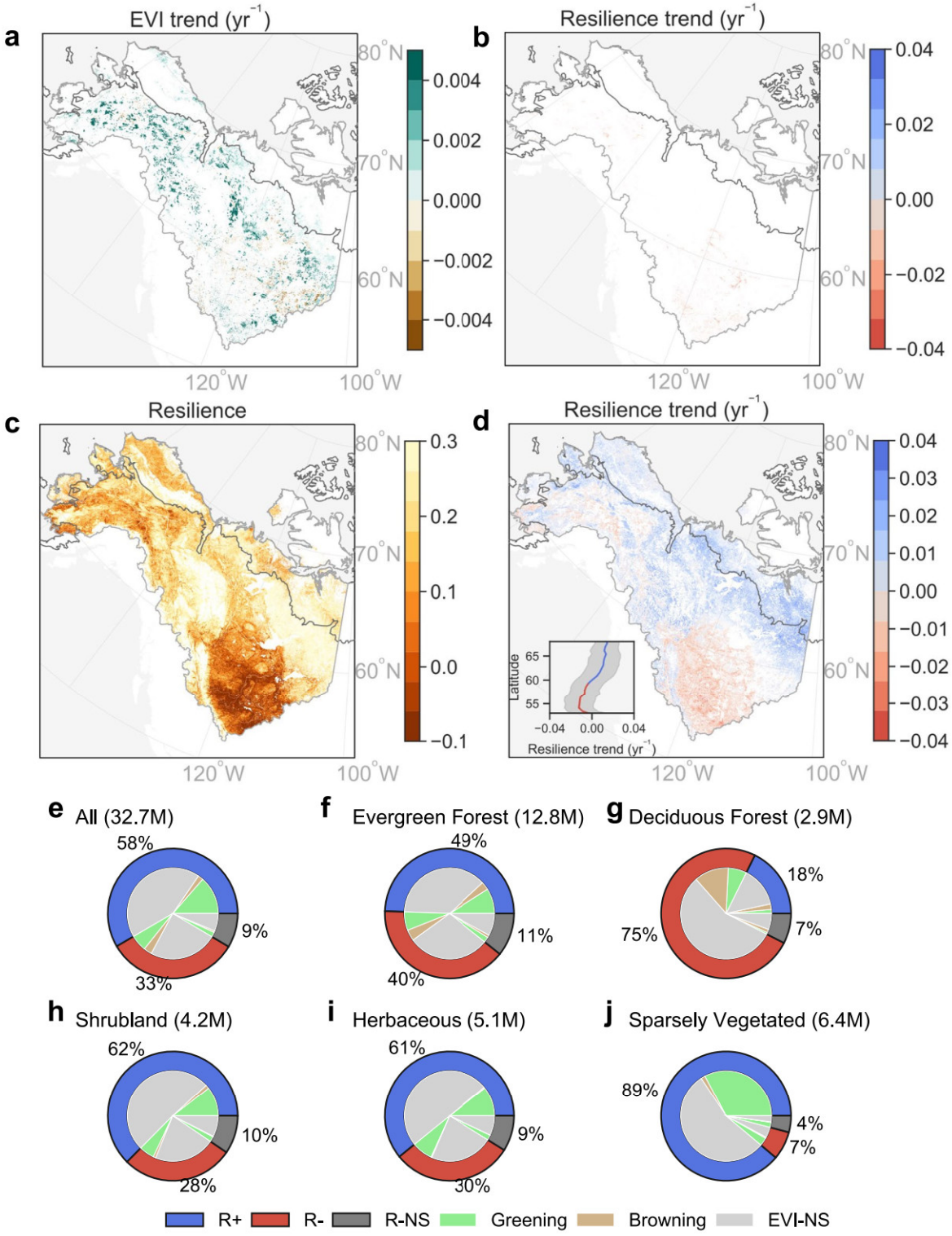

Extended Data Fig. 4 | Greening is not always associated with enhanced vegetation resilience. **(a)** Statistically significant (two-sided *t* test $\alpha = 0.05$) greening and browning locations. **(b)** Greening areas with decreasing resilience. Colours represent long-term resilience (negative lag-1 autocorrelation) trends. **(c)** The spatial pattern of vegetation resilience averaged from 2003 to 2019 across the ABoVE core domain. **(d)** Similar to Fig. 1 in the main text, the map shows the trend of resilience for areas without land cover change or fire disturbances. The inset shows the latitudinal variation of resilience trend with a bin size of 0.75°, where the line and gray band denote the mean and the standard variation, respectively. **(e)-(j)** Similar to Fig. 2 in the main text, the outer pie shows the areal fractions of significantly (two-sided *t* test $\alpha = 0.05$) increased (R +), significantly decreased (R-), and non-significant (R-NS) resilience trend among all vegetated areas without land cover change or fire disturbances (**e**) and the major land cover types, including evergreen forest (**f**), deciduous forest (**g**), shrubland (**h**), herbaceous (**i**) and sparsely vegetated (**j**). The nested inner pie shows the areal fractions of significant greening, browning, and non-significant (EVI-NS) greenness trend within each resilience trend group (outer pie). The number of pixels in each panel is noted in round brackets.

https://doi.org/10.1038/s41559-024-02551-0

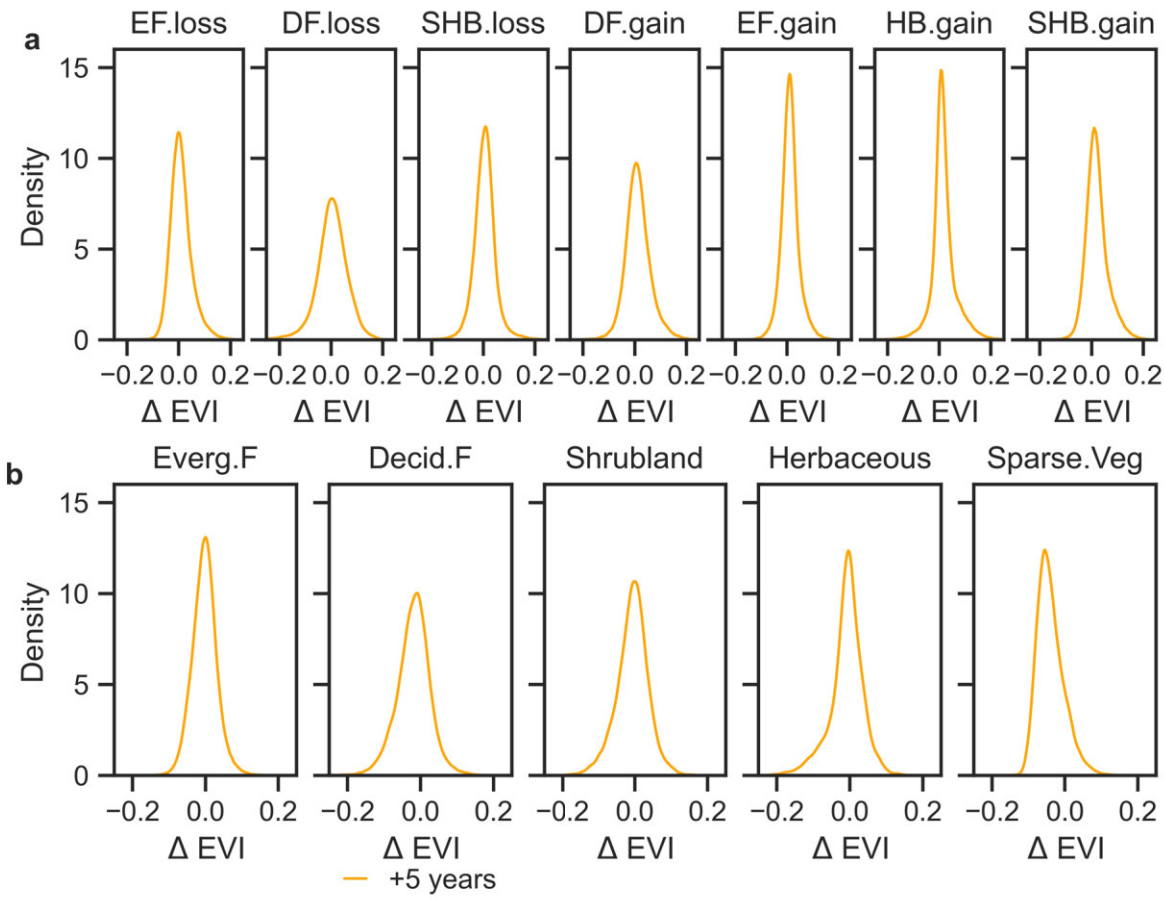

Extended Data Fig. 5 | Heterogeneous changes of EVI equilibrium after land cover changes and fires. (**a**) Probability distributions of EVI equilibrium change (Δ EVI) from the equilibrium before land cover change (LCC) to that five years after, grouped by LCC types. (**b**) Probability distributions of Δ EVI from the equilibrium before fire to that five years after, grouped by land cover types. The equilibrium state is quantified by the local mean component in the Bayesian dynamic linear model. The equilibrium before LCC and fire is quantified using the averaged local mean from 2003 till five years prior to LCC or fire.

https://doi.org/10.1038/s41559-024-02551-0

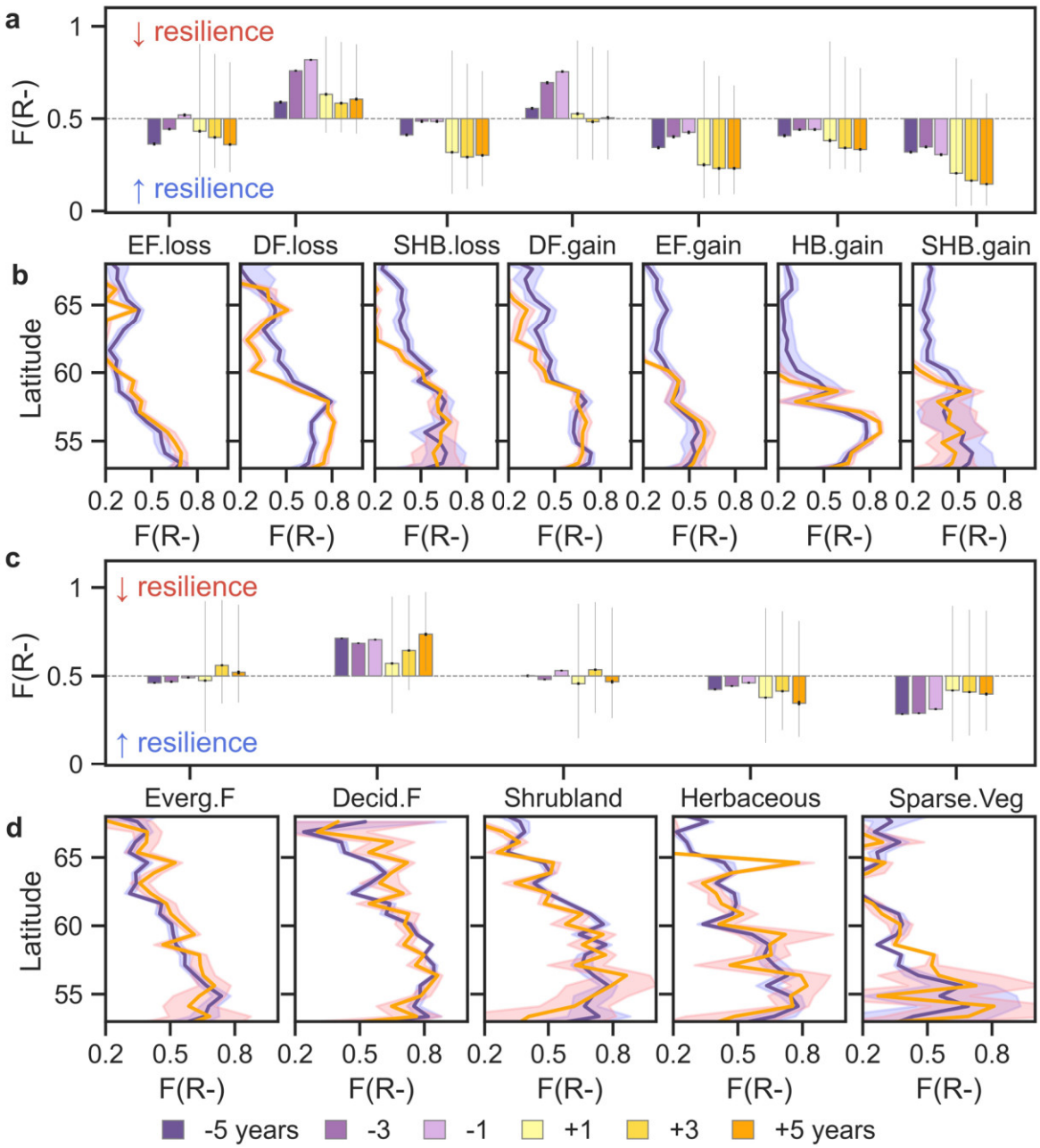

Extended Data Fig. 6 | Uncertainty of resilience change after land cover changes and fires. Same as Fig. 4 in the main text, except that results are from an alternative version of the Bayesian dynamic linear model with intervention at the time of climate-driven land cover change (LCC) or fire (Methods). **(a)** The fraction of resilience lower than the baseline (F(R-)) between five years before and after LCC, grouped by LCC types, that is evergreen forest loss (EF.loss), deciduous forest loss (DF.loss), shrub loss (SHB.loss), deciduous forest gain (DF.gain), evergreen forest gain (EF.gain), herbaceous gain (HB.gain) and shrub gain (SHB.gain). An F(R-) > 0.5 indicates that most pixels in this group experienced reduced resilience. (**b**) The latitudinal variation of F(R-) grouped by a bin size of 0.75° for each LCC type. (**c**) F(R-) before and after fires grouped by the pre-fire land cover types and (**d**) the corresponding latitudinal variation, similar to (**a**) and (**b**). The colours represent five years before (-5) and after (+5) the land cover change or fire, and so forth. F(R-) was calculated by comparing resilience (posterior mean) in the target year to the temporal baseline, that is, the resilience at the same location averaged between 2003 to five years before changes. The bar height in **(a)** and **(c)** is the mean F(R-) across 100 sets of bootstrapping pixels for each group (n = 10,000 for each set). The thick black vertical line shows the standard deviation, suggesting robust estimates across sampled pixels. The lower/upper end of the thin grey vertical line is F(R-) quantified by comparing the upper/lower boundary of resilience (posterior mean plus/minus posterior standard deviation) to the abovementioned baseline, indicating large posterior range of resilience estimates post changes. The lines and shaded bands in (**b**) and (**d**) show the mean and standard deviation of F(R-) from 100 bootstrap resampling.

https://doi.org/10.1038/s41559-024-02551-0

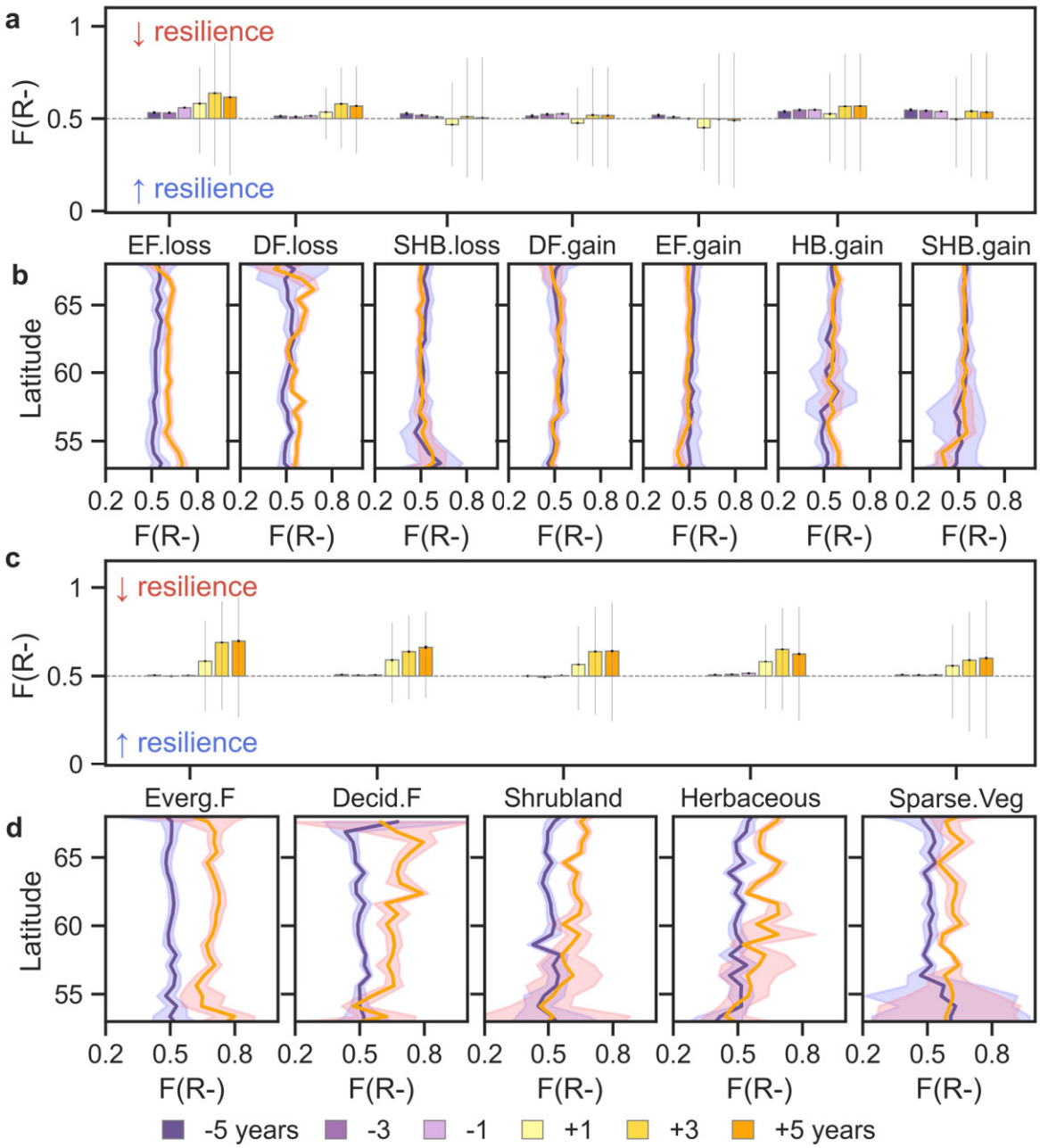

Extended Data Fig. 7 | Changes of resilience before and after land cover changes and fire with respect to the spatial baseline. (a) The fraction of resilience lower than the baseline (F(R-)) between five years before and after climate-driven land cover change (LCC), grouped by LCC types, that is evergreen forest loss (EF.loss), deciduous forest loss (DF.loss), shrub loss (SHB.loss), deciduous forest gain (DF.gain), evergreen forest gain (EF.gain), herbaceous gain (HB.gain) and shrub gain (SHB.gain). An F(R-) > 0.5 indicates that most pixels in this group experienced reduced resilience. (**b**) The latitudinal variation of F(R-) grouped by a bin size of 0.75° for each LCC type. (**c**) F(R-) before and after fires grouped by the pre-fire land cover types and (**d**) the corresponding latitudinal variation, similar to (**a**) and (**b**). The colours represent five years before (-5) and after (+5) the land cover change or fire, and so forth. F(R-) was calculated by comparing resilience (posterior mean) in the target year to the spatial baseline, that is, the spatially averaged resilience (posterior mean) across nearby similar pixels in the same year of the abrupt change, corrected by the spatial difference between the initial resilience conditions. The bar height in (**a**) and (**c**) is the mean F(R-) across 100 sets of bootstrapping pixels for each group (n = 10,000 for each set). The thick black vertical line shows the standard deviation, suggesting robust estimates across sampled pixels. The lower/upper end of the thin grey vertical line is F(R-) quantified by comparing the upper/lower boundary of resilience (posterior mean plus/minus posterior standard deviation) to the abovementioned baseline, indicating large posterior range of resilience estimates post changes. The lines and shaded bands in (**b**) and (**d**) show the mean and standard deviation of F(R-) from 100 bootstrap resampling.

https://doi.org/10.1038/s41559-024-02551-0

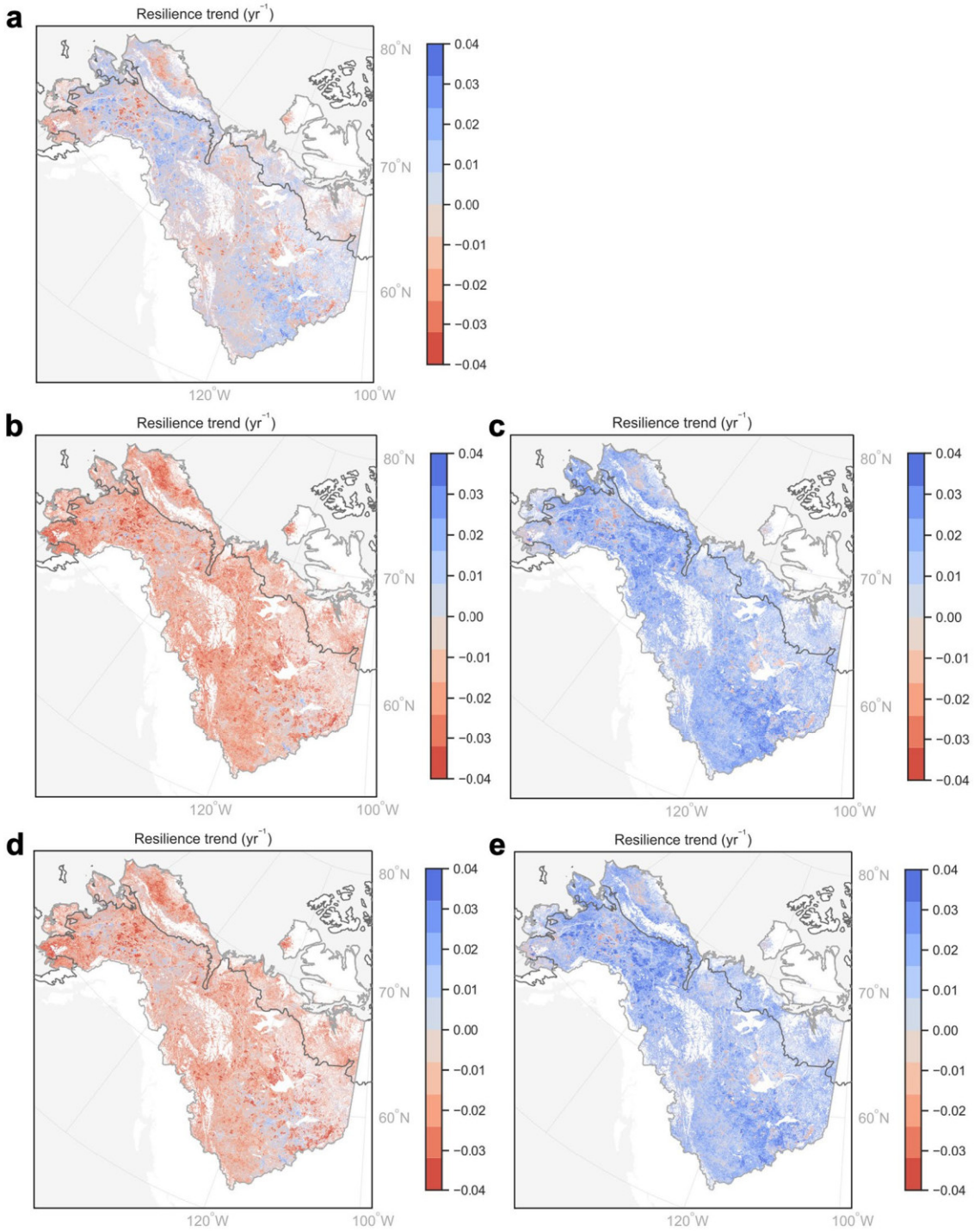

Extended Data Fig. 8 | Resilience trend calculated using a moving window approach exhibits large uncertainties. (a) The vegetation resilience trend calculated by replicating the method as described in ref. 41 using the EVI data same as in this work during 2000–2019 across the ABoVE core domain. Key steps include deseasonalizing and detrending the 16-day EVI time series, calculating the long-term lag-1 autocorrelation of EVI (TAC), using long-term average forest density, background climate, climate variability and autocorrelation in climate as predictors (X) of a Random Forest regression model to model TAC, calculating annual lag-1 autocorrelation of EVI (TAC^t) and predictors (X^t) within a 3-year moving window, calculating the impact of autocorrelation in climate on the lag-1 autocorrelation of EVI ($TAC^t|X_{ac}$) using the Random Forest regression model ($RF(X^t)$-$RF(X_{ac}^{\ t}, X_{ac}^{\ 2000})$), factoring out the impact of autocorrelation in climate from the annual lag-1 autocorrelation of EVI (TAC^t-$TAC^t|X_{ac}$), and computing the linear trend of the resulting enhanced annual autocorrelation of EVI. **(b)-(c)**, The 5th percentile **(b)** and 95th percentile **(c)** of vegetation resilience trend from 100 times of pairwise bootstrapping the raw annual time series of lag-1 autocorrelation of EVI (TAC^t) with replacement. **(d)-(e)**,The 5th percentile **(d)** and 95th percentile **(e)** of vegetation resilience trend from sampling the impact of autocorrelation in climate on the autocorrelation of EVI ($TAC^t|X_{ac}$) 100 times from a Gaussian distribution centered around the prediction of the random forest regression model with a standard deviation calculated from the regression residuals. The difference between **(b)** and **(c)** indicates a large uncertainty of resilience trend arising from estimates of annual lag-1 autocorrelation, likely caused by a large fraction of missing data in high latitude regions. The difference between **(d)** and **(e)** indicates a large uncertainty due to a much lower explicative power of the Random Forest regression model in this region (30%) compared to that in the original global scale study (87%).

https://doi.org/10.1038/s41559-024-02551-0

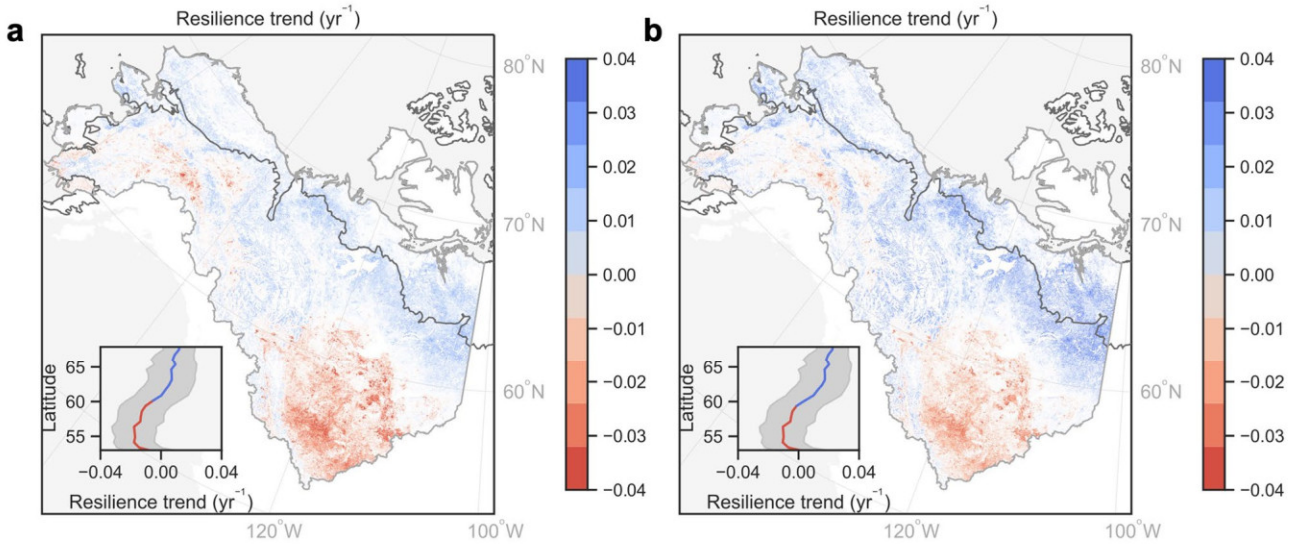

Extended Data Fig. 9 | The uncertainty of resilience trend due to the uncertainty of posterior estimates of autocorrelation using the Bayesian dynamic linear model. The 5th percentile **(a)** and 95th percentile **(b)** of vegetation resilience (negative lag-1 EVI autocorrelation) trend during 2000–2019 across the ABoVE core domain with a discounting parameter of 0.98. Legends and abbreviations are the same as in Fig. 1.

https://doi.org/10.1038/s41559-024-02551-0

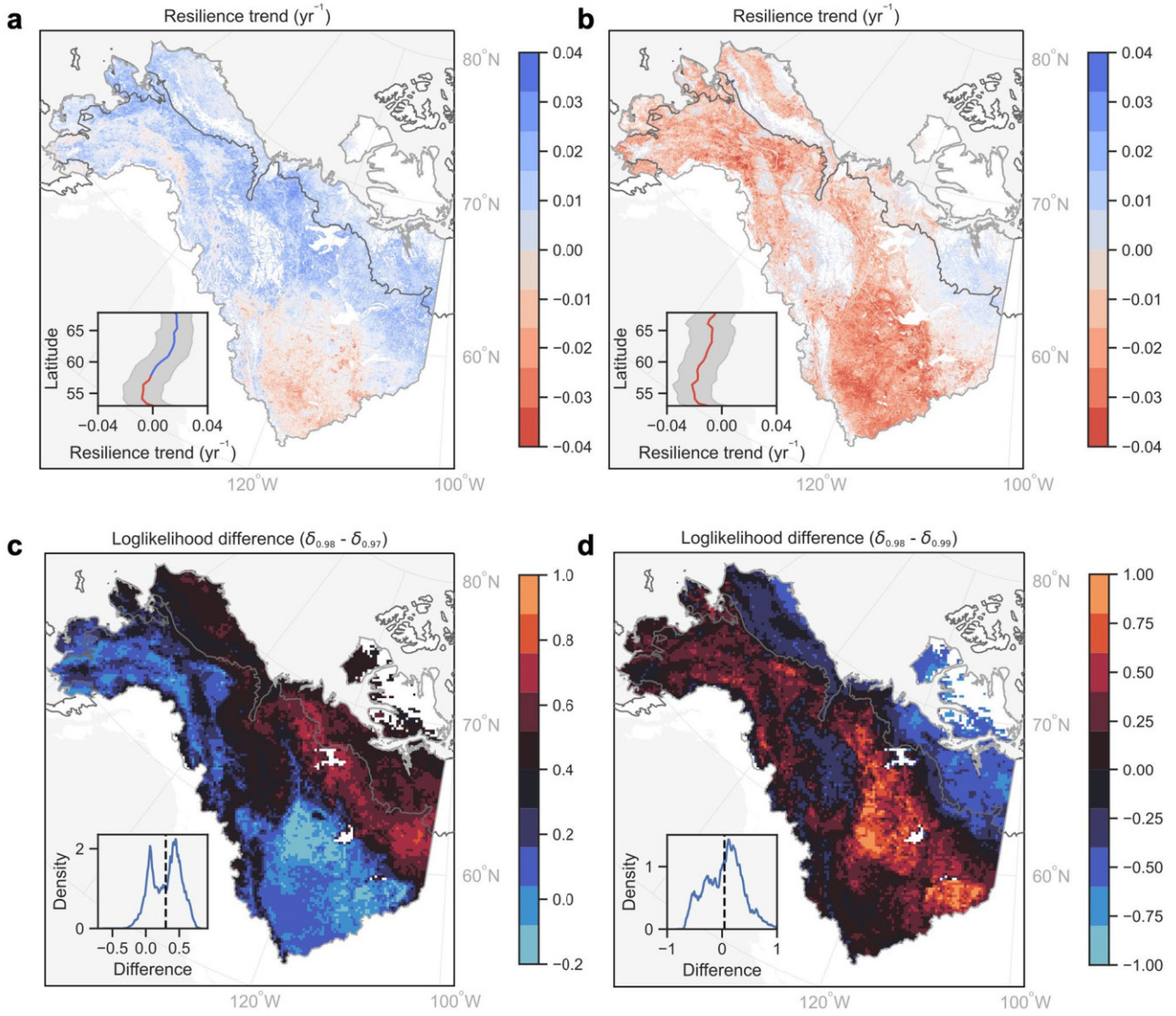

Extended Data Fig. 10 | The uncertainty of resilience trend due to the choice of the discounting parameter controlling the information decay rate. Spatial patterns of resilience trend, same as Fig. 1 (default discounting parameter $\delta_{0.98}$), but with alternative discounting parameters of $\delta_{0.97}$ (**a**) and $\delta_{0.99}$ (**b**), respectively. Model performances are measured by log-likelihoods and compared between the alternative parameters and the default, shown as differenced maps and density plots, the black dashed line shows the average log-likelihood difference ($\delta_{0.98}$-$\delta_{0.97}$ in **c**; $\delta_{0.98}$-$\delta_{0.99}$ in **d**). The model performs the best using $\delta_{0.98}$, according to the average log-likelihood, which is used as the default in Fig. 1. All three discounting parameters result in consistent trend directions in southern boreal forests, supporting the robustness of reduced resilience in boreal forests. The model suggests relatively lower confidence in the increasing resilience in the Arctic tundra given $\delta_{0.99}$ yields reverse trends from $\delta_{0.98}$ and $\delta_{0.97}$, in despite of a similar model likelihood as that using $\delta_{0.98}$ (**d**).

nature portfolio

Corresponding author(s): Yanlan Liu

Last updated by author(s): 08/13/2024

Reporting Summary

Nature Portfolio wishes to improve the reproducibility of the work that we publish. This form provides structure for consistency and transparency in reporting. For further information on Nature Portfolio policies, see our Editorial Policies and the Editorial Policy Checklist.

Statistics

For all statistical analyses, confirm that the following items are present in the figure legend, table legend, main text, or Methods section.

n/a	Confirmed
☐	☒ The exact sample size (*n*) for each experimental group/condition, given as a discrete number and unit of measurement
☒	☐ A statement on whether measurements were taken from distinct samples or whether the same sample was measured repeatedly
☐	☒ The statistical test(s) used AND whether they are one- or two-sided *Only common tests should be described solely by name; describe more complex techniques in the Methods section.*
☐	☒ A description of all covariates tested
☐	☒ A description of any assumptions or corrections, such as tests of normality and adjustment for multiple comparisons
☐	☒ A full description of the statistical parameters including central tendency (e.g. means) or other basic estimates (e.g. regression coefficient) AND variation (e.g. standard deviation) or associated estimates of uncertainty (e.g. confidence intervals)
☒	☐ For null hypothesis testing, the test statistic (e.g. *F*, *t*, *r*) with confidence intervals, effect sizes, degrees of freedom and *P* value noted *Give P values as exact values whenever suitable.*
☐	☒ For Bayesian analysis, information on the choice of priors and Markov chain Monte Carlo settings
☒	☐ For hierarchical and complex designs, identification of the appropriate level for tests and full reporting of outcomes
☒	☐ Estimates of effect sizes (e.g. Cohen's *d*, Pearson's *r*), indicating how they were calculated

Our web collection on statistics for biologists contains articles on many of the points above.

Software and code

Policy information about availability of computer code

Data collection	No software was used for data collection.
Data analysis	The Python package statsmodels (version 0.12.2) was used in linear regression. The python package RichDEM (0.3.4) was used to derive slope and aspect from elevation. The R packages randomForest (version 4.7-1.1) , caret (version 6.0-92), and pdp (version 0.8.0) were used to identify critical environmental controls on resilience trend. Codes are available at Zenodo (http://doi.org/10.5281/zenodo.10719618)

For manuscripts utilizing custom algorithms or software that are central to the research but not yet described in published literature, software must be made available to editors and reviewers. We strongly encourage code deposition in a community repository (e.g. GitHub). See the Nature Portfolio guidelines for submitting code & software for further information.

Data

Policy information about availability of data

All manuscripts must include a data availability statement. This statement should provide the following information, where applicable:

- Accession codes, unique identifiers, or web links for publicly available datasets
- A description of any restrictions on data availability
- For clinical datasets or third party data, please ensure that the statement adheres to our policy

The annual resilience maps produced in this study are archived and freely available at the NASA ORNL Active Archive Center (DAAC) (https://doi.org/10.3334/ORNLDAAC/2374)

All datasets used in this study are publicly available.
The MODIS EVI dataset is available at https://lpdaac.usgs.gov/products/mod13q1v061/.
The annual land-cover product is available at https://daac.ornl.gov/ABOVE/guides/Annual_Landcover_ABoVE.html.
The climate conditions and the application to downscale (ClimateNA) is available at https://climatena.ca/.
The disturbances datasets are available at https://daac.ornl.gov/ABOVE/guides/ABoVE_ForestDisturbance_Agents.html, and https://daac.ornl.gov/ABOVE/guides/Burned_Area_Depth_AK_CA.html.
Active layer thickness data are available at https://catalogue.ceda.ac.uk/uuid/67a3f8c8dc914ef99f7f08eb0d997e23.
The ASTER DEM is available at https://lpdaac.usgs.gov/products/astgtmv003/.
The soil moisture data are from https://catalogue.ceda.ac.uk/uuid/43d73291472444e6b9c2d2420dbad7d6.
The soil nitrogen data are from https://www.isric.org/explore/soilgrids.

Research involving human participants, their data, or biological material

Policy information about studies with human participants or human data. See also policy information about sex, gender (identity/presentation), and sexual orientation and race, ethnicity and racism.

Reporting on sex and gender	N/A
Reporting on race, ethnicity, or other socially relevant groupings	N/A
Population characteristics	N/A
Recruitment	N/A
Ethics oversight	N/A

Note that full information on the approval of the study protocol must also be provided in the manuscript.

Field-specific reporting

Please select the one below that is the best fit for your research. If you are not sure, read the appropriate sections before making your selection.

☐ Life sciences ☐ Behavioural & social sciences ☒ Ecological, evolutionary & environmental sciences

For a reference copy of the document with all sections, see nature.com/documents/nr-reporting-summary-flat.pdf

Ecological, evolutionary & environmental sciences study design

All studies must disclose on these points even when the disclosure is negative.

Study description	We quantified time-varying vegetation resilience using temporal autocorrelation of remotely sensed greenness during 2000–2019 across Alaska and Western Canada. We further studied the critical environmental controls of resilience trend and temporal trajectory of vegetation resilience before/after land cover changes or fire disturbances.
Research sample	We analyzed the entire vegetated region with valid values in necessary datasets in the ABoVE core study domain. The area of interest includes 39.6M 300 m by 300 m pixels.
Sampling strategy	For selecting informative climate variables using multivariate regression and resilience estimation using Bayesian dynamic linear model, all available pixels are used. For identifying critical environmental controls on resilience trend, 100 datasets (each with 56.7K pixels) were randomly selected from all 31.0M vegetated pixels without recorded land cover change or disturbance. For investigating resilience variation before/after land cover change or fire disturbances, 700 datasets (each with 10K pixels for each of the seven land cover change groups) were sampled from 2.6M pixels with climate-driven land cover change, and 500 datasets (each with 10K pixels for each of the five land cover types) were sampled from 2.8 million pixels with fire.
Data collection	All datasets described in the data availability statement were downloaded from the URL sources by Yue Zhang.
Timing and spatial scale	The EVI data have a spatial resolution of 250 m and a temporal resolution of 16-day span across 2000-2019. The annual land cover data have a spatial resolution of 30 m span across 2000-2019. The annual disturbance agents data have a spatial resolution of 30 m span across 2000-2012. The annual burned area and depth data have a spatial resolution of 500 m span across 2001-2019. The time-invariant elevation data have a spatial resolution of 30 m. The time-invariant SoilGrids data have a spatial resolution of 250 m. The annual active layer thickness have a spatial resolution of 900 m. The daily soil moisture data have a spatial resolution of 25 km. The annual land cover data have a spatial resolution of 30 m. The monthly ClimateNA data have a spatial resolution of 4 km.
Data exclusions	Non-vegetated areas and vegetated areas with low valid data availability were excluded from analysis.

Reproducibility	All attempts to repeat the analysis were successful.
Randomization	Randomization was achieved through setting random seeds in the Python coding environment.
Blinding	Blinding was not relevant.

Did the study involve field work? ☐ Yes ☒ No

Reporting for specific materials, systems and methods

We require information from authors about some types of materials, experimental systems and methods used in many studies. Here, indicate whether each material, system or method listed is relevant to your study. If you are not sure if a list item applies to your research, read the appropriate section before selecting a response.

Materials & experimental systems

n/a	Involved in the study
☒	☐ Antibodies
☒	☐ Eukaryotic cell lines
☒	☐ Palaeontology and archaeology
☒	☐ Animals and other organisms
☒	☐ Clinical data
☒	☐ Dual use research of concern
☒	☐ Plants

Methods

n/a	Involved in the study
☒	☐ ChIP-seq
☒	☐ Flow cytometry
☒	☐ MRI-based neuroimaging

Plants

Seed stocks	N/A
Novel plant genotypes	N/A
Authentication	N/A